JMEPEG
https://doi.org/10.1007/s11665-024-09801-z

1059-9495/$19.00

REVIEW

Elemental Composition, Phase Diagram, Microstructure, Fabrication Processes, and Mechanical Properties of Ti_2AlNb Alloy: A Review

Yanqi Fu and Zimu Su

Submitted: 1 July 2023 / Revised: 11 May 2024 / Accepted: 27 May 2024

The Ti_2AlNb alloy is a refractory material with the potential to replace Ni-based alloys in the manufacturing process of aerospace engines. However, the development of this alloy is still in the research stage, requiring further investigation to promote its industrial application. Therefore, this paper provides an overview of the alloy, starting from its elemental composition and encompassing its microstructural morphology, fabrication processes, and mechanical properties. First, this paper presents the nine common alloying elements (Al, Nb, Mo, Zr, Fe, V, W, Ta, and Si), which play various roles in determining the alloy's microstructure and mechanical performance. Then, the paper presents three typical microstructures and the corresponding microstructure regulation processes, providing references for microstructure regulation. In the regulation process, although there are seven manufacturing processes (Casting, Forming under pressure, Machining, Welding and joining, Powder metallurgy, Additive manufacturing, and Surface treatment) currently applied to the industrialization of this alloy, certain shortcomings still exist, indicating significant research opportunities. Finally, the paper summarizes the relationships between the alloy's typical microstructures and its mechanical properties. In conclusion, the work presented in this paper offers a clear reference for advancing the industrial application of the alloy and encourages future researchers to contribute to the further development of this field based on the foundation established by this review.

Keywords elemental composition, fabrication processes, microstructure, mechanical properties, phase diagram, Ti_2AlNb

1. Introduction

Since the incorporation of Nb into Ti-Al alloys, the newly discovered O-phase Ti_2AlNb alloy (Ref 1) has emerged as a viable material for advanced aerospace engines, owing to its superior high-temperature strength, excellent oxidation resistance, outstanding creep resistance, and microstructural stability. However, the application of this alloy in complex service environments such as aerospace engines is limited by its coarse grain size, complex constituent phases, and intricate phase interactions. The further development of this alloy is closely associated with advancements in its elemental composition, microstructural characteristics, fabrication processes, and mechanical properties. Meanwhile, while there are already some review articles (Ref 2-4) on Ti_2AlNb alloys, these publications typically have a narrow scope, focusing primarily on specific domains of research, thus failing to provide a sufficiently broad knowledge base. This limited coverage poses a hurdle for researchers who are newly entering this field, impeding their learning process. They struggle to attain a comprehensive understanding and are hindered from delving deeply into various facets of the alloy and its potential value across diverse applications. Hence, there exists a compelling need for a more comprehensive and inclusive review article. Such a publication would serve to assist novice researchers in establishing a robust foundation, ultimately leading to greater success in both research endeavors and practical applications. The dissemination of such an article would contribute significantly to advancing our understanding of Ti_2AlNb alloys and promoting further research in this domain. Therefore, this article provides a comprehensive review of this alloy's relevant aspects, serving as a valuable reference for future researchers, as shown in Fig. 1.

2. Elemental Composition and Its Impacts of Ti_2AlNb Alloy

The elemental composition (in terms of mole fraction) of Ti_2AlNb alloy is primarily dominated by Ti-(18-30%)Al-(12.5-30%)Nb. In comparison to conventional Ti-Al alloys, the addition of Nb leads to the precipitation of a new phase, denoted as the O phase, within Ti_2AlNb alloy. In the academic community, researchers have classified the developmental progression of Ti_2AlNb alloy into two generations based on the varying content of Nb. When the molar fraction of Nb is less than 25%, the phase composition of Ti_2AlNb alloy after heat treatment in the three-phase region (β/B2 + α_2 + O) is

Yanqi Fu, School of Material Science and Engineering, Shanghai Jiao Tong University, 800 Dongchuan Road, Shanghai 200240, China; and **Zimu Su**, Department of Civil and Environmental Engineering, Vanderbilt University, Nashville TN37235. Contact e-mail: fuyanqi@sjtu.edu.cn.

Published online: 08 July 2024

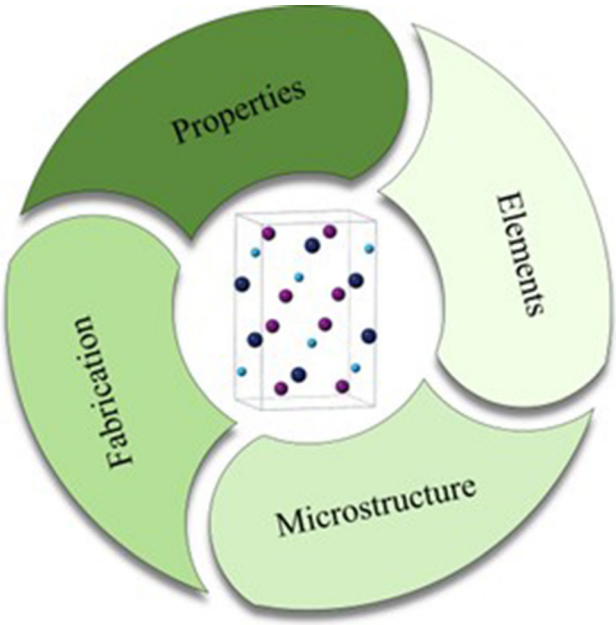

Fig. 1 Structure of the review article, including Alloy elements, Microstructure, Fabrication processes, and Mechanical properties

denoted as β/B2 + α_2 + O, and at this point, the alloy is referred to as a first-generation Ti_2AlNb alloy. At this juncture, the nominal composition of the aforementioned alloy is designated as Ti-25Al-17Nb, Ti-21Al-22Nb, and Ti-22Al-23Nb. When the molar fraction of Nb exceeds or equals 25%, the B2 + O phase alloy obtained after heat treatment in the two-phase region (B2 + O) is referred to as the second-generation O phase alloy. Its nominal composition is designated as Ti-22Al-25Nb and Ti-22Al-27Nb.

During the development of Ti_2AlNb alloy, variations in the content of the three constituent elements (Ti, Al, and Nb) result in divergent mechanical properties. In addition to modulating the content of the three constituent elements, the incorporation of other alloying elements (Mo, Zr, Fe, Ta, W, Si, V, among others) serves as a crucial approach to enhance the comprehensive performance of Ti_2AlNb alloy. As shown in Fig. 2, primarily, the incorporation of these elements into Ti_2AlNb alloy manifests solid solution strengthening (Si, Fe, Al, V, Zr) and fine-grain strengthening (W, Mo, Nb, Ta), thereby enhancing its mechanical properties. Subsequently, the inclusion of these alloying elements in Ti_2AlNb alloy exerts diverse effects on other material properties, such as oxidation resistance, tensile strength, elastic modulus, plasticity, among others. The effects exerted by different elements on Ti_2AlNb alloy can be summarized as follows.

Al: Increasing the content of Al enhances the alloy's oxidation resistance, tensile strength, and elastic modulus, while concurrently diminishing its ductility and fracture toughness (Ref 5).

Nb: Increasing the Nb content (15-27%) enhances the strength, creep resistance, and fracture toughness of the alloy (Ref 6). However, the elevation of Nb content leads to an increase in alloy density, a reduction in oxidation resistance (Ref 7), and hampers the uniform distribution of alloy constituents during ingot solidification, thereby exacerbating the challenges in the melting process.

Mo and **Zr**: By incorporating Mo and Zr as partial substitutes for Nb, it is possible to refine the microstructure of the O phase lamellar (Ref 8), ensuring that the alloy maintains high oxidation resistance (Ref 9), creep resistance (Ref 10, 11), and excellent high-temperature performance without compromising its yield strength and plasticity (Ref 10).

Fe: The addition of Fe as a partial substitute for Nb leads to an enhancement in the high-temperature tensile yield strength and ultimate tensile strength (Ref 11).

V: The inclusion of V increases room-temperature ductility, also at the cost of reduced strength and oxidation resistance (Ref 12).

W: The addition of W refines the lamellar microstructure, thereby enhancing the high-temperature tensile strength (Ref 13).

Ta: The substitution of Nb with Ta increases the strength of the O phase and B2 phase, while also enhancing the strength of the B2 + O matrix through the refinement of the O phase lamellar thickness. Furthermore, it maintains high-temperature tensile ductility. Moreover, it can raise the β/B2 phase transformation temperature.

Si: The addition of 0.3 to 0.9% (molar fraction) Si improves the alloy's oxidation resistance at 650 and 750 °C, resulting in an approximate 20% increase in creep resistance. However, it concurrently decreases room-temperature ductility and fracture toughness (Ref 7).

3. Ti-Al-Nb Alloy Phase Diagram

3.1 Isothermal Phase Diagrams

In recent years, numerous researchers have investigated the ternary isothermal phase diagram of Ti-Al-Nb alloys at elevated temperatures, such as 1000, 1150, 1300, 1400 °C, etc (Ref 14-18). Despite extensive research efforts on Ti-Al-Nb ternary alloy phase diagrams, several challenges and limitations still exist in the current work, including insufficient and inaccurate data. As depicted in Fig. 3, among all the established ternary phase diagrams, the phase diagram proposed by Witusiewicz (Ref 17) and Cupid (Ref 19) exhibits the highest accuracy, incorporating the O-Ti_2AlNb and ω_0-Ti_4NbAl_3 which cannot be predicted by binary alloy phase diagrams. Furthermore, Xu et al. (Ref 15, 16, 20) employed novel characterization methods (SEM, EBSD, EPMA, DSC, et al) to systematically investigate the ternary alloy phase diagrams under high-temperature conditions. However, substantive research regarding the precipitation of the O phase in Ti-Al-Nb ternary alloys remains lacking, despite the substantial efforts devoted by researchers to study ternary alloy phase diagrams.

3.2 Pseudo-Binary Phase Diagram

In the industrial sector, as the application of O-phase titanium alloys becomes increasingly widespread, numerous researchers have shifted their focus to pseudo-binary phase diagrams of Ti-(22,25)Al-*x*Nb alloys for the sake of convenience in studying the related issues. As shown in Fig. 4, the pseudo-binary phase diagram has undergone extensive research and continuous improvements by various investigators (Ref 21, 22). It can be observed that the Nb and Al contents have a significant influence on the temperature range of the phase regions. The typical phase regions in both diagrams include B2/

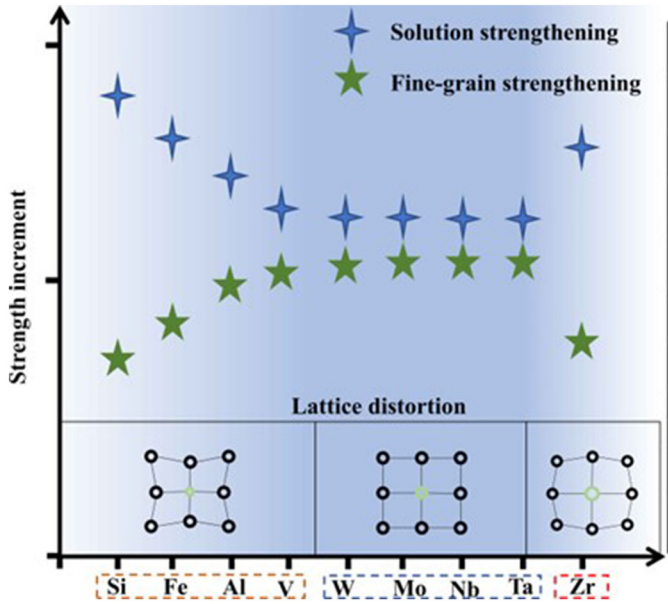

Atom	Radius (pm)
Si	117
Fe	117
Al	118
V	122
W	130
Mo	130
Nb	134
Ta	134
Zr	145

Fig. 2 Strengthening mechanisms of different elements in Ti_2AlNb alloy

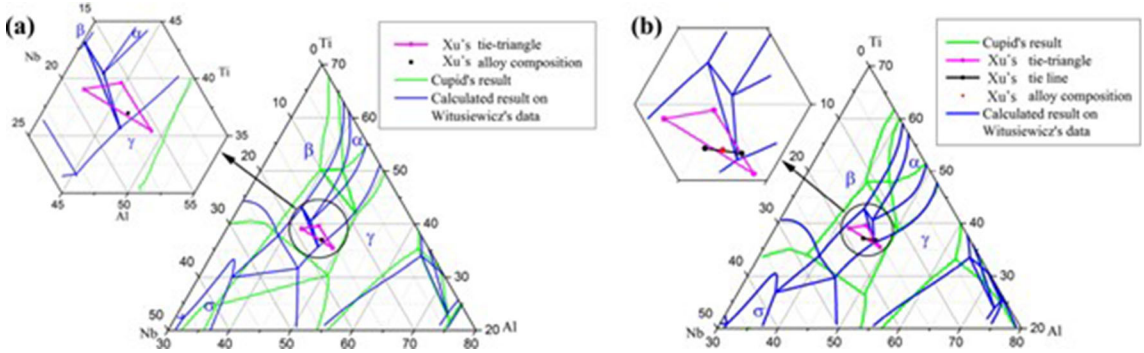

Fig. 3 Isothermal phase diagram at (a) 1300 °C, and (b) 1400 °C obtained from Witusiewicz (Ref 17) and Cupid (Ref 19) and the tie-triangle identified in Xu's research (Ref 20). Reprinted from *Journal of Materials Science & Technology,* Vol 80, Hongyu Zhang, Na Yan, Hongyan Liang, Yongchang Liu, Phase transformation and microstructure control of Ti_2AlNb-based alloys: A review, Pages No. 203-216, Copyright 2021, with permission from Elsevier

β, α_2 + B2/β, α_2 + O + B2/β, B2/β + O, and O phase regions. When the atomic fraction of Al is 22%, the range of the B2 + O phase region expands with increasing Nb content. This inevitably leads to an increase in alloy density. To mitigate excessive alloy density and achieve an extended range of the B2 + O phase region, a second-generation Ti_2AlNb alloy (Ti-22Al-25Nb) has been developed for engineering production. When the molar fraction of Al in the alloy is 25%, even with the same content of Nb element, there can be significant variations in the phase region range within the phase diagrams.

Taking the case of Nb element with a molar fraction of 25%, the Ti_2AlNb alloy undergoes a typical phase transformation process when cooled from a high-temperature single-phase region to room temperature.

B2 → α_2: When the alloy is cooled from a high-temperature single-phase region (B2/β phase) to a two-phase region (B2/β + α_2 phases), the α_2 phase precipitates from the matrix phase (B2/β phase) through either shear or diffusion. The B2 matrix phase and the precipitated α_2 phase maintain an orientation relationship (Ref 21): $(0001)_{\alpha 2}//(110)_{B2}$, $[11\ \bar{2}\ 0]_{\alpha 2}//[1\ \bar{1}\ 1]_{B2}$.

Peritectoid reaction: When the alloy is cooled from the two-phase region (B2/β + O phases) to the three-phase region (B2/β + α_2 + O phases), the reaction B2 + α_2 → O occurs.

As the temperature continues to decrease, the alloy undergoes the reaction: B2 → B2 + O.

When the alloy's Al content increases from 22 to 25%, even with the same Nb content, the phase transformation process during cooling from the high-temperature single-phase region varies significantly. This observation suggests that the Al and Nb content play a crucial role in the phase transformation during the cooling process within the Ti_2AlNb alloy.

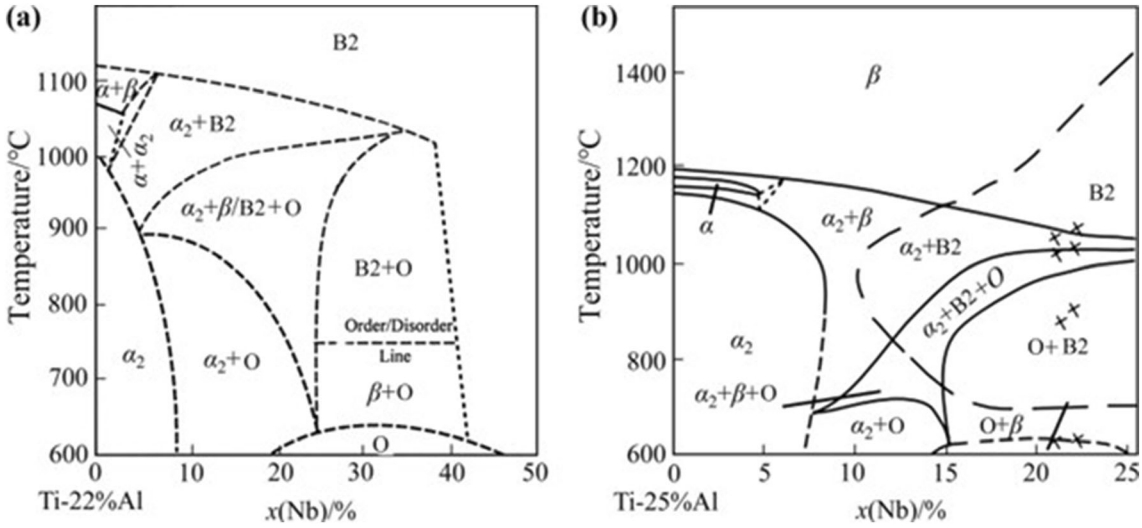

Fig. 4 Pseudo-binary phase diagram of Ti-Al-Nb alloy: (a) Ti-22Al-*x*Nb (Ref 21). (b) Ti-25Al-*x*Nb (Ref 22). (a) Reprinted from *Journal of Materials Science & Technology,* Vol 80, Hongyu Zhang, Na Yan, Hongyan Liang, Yongchang Liu, Phase transformation and microstructure control of Ti_2AlNb-based alloys: A review, Pages No. 203-216, Copyright 2021, with permission from Elsevier. (b) Reprinted with permission from N. V. Kazantseva et al, Study of the Ti-Al-Nb phase diagram, *Physics of Metals and Metallography,* volume 102, 189-180, 2006, Springer Nature

4. Phase Composition, Phase Formation Mechanisms, and Typical Microstructure Characteristics of Ti_2AlNb Alloy

4.1 Phase Composition

According to numerous previous studies, it has been demonstrated that there are three primary phases present in this alloy, namely the O phase, B2 phase, and α_2 phase. The lattice parameters of these three phases are provided in Table 1.

According to extensive research, the most significant constituent phase of titanium alloys is the B2/β phase. This phase adopts a body-centered cubic (bcc) structure with a space group of Pm $\bar{3}$ m, which belongs to the CsCl-type structure, as shown in Fig. 5(a). The lattice of this structure contains a significant number of interstitial sites, allowing for the incorporation of a large amount of elements. The variation in element content leads to significant changes in the composition of the B2 phase. The β phase represents the disordered form of the B2 phase, characterized by a disordered bcc structure. Its space group is Im $\bar{3}$ m. With increasing temperature, the internally ordered B2 phase within the alloy transforms into the disordered β phase (Ref 24). The temperature at which the transition from the ordered phase to the disordered phase occurs remains constant under the condition of unchanged element types and contents within the alloy. However, the transition temperature (≈1383 K) between the ordered and disordered phases varies with changes in element types and contents (Ref 2, 24, 25).

In traditional titanium alloys, the α phase is an important strengthening phase. With the development of titanium alloys, the newly developed Ti_2AlNb alloy also contains the α_2 phase, which acts as a hardening phase within the material. The crystal structure of this phase is hexagonal close-packed (HCP), with a space group of $P6_3/mmc$, as shown in Fig. 5(b). In traditional titanium alloys, the chemical composition of this phase is Ti_3Al. However, with the addition of Nb elements in traditional titanium alloys, Ti and Al atoms arrange themselves in a specific order within the lattice, while Nb atoms randomly occupy the sub-lattice of Ti atoms (Ref 27). Due to its limited slip systems, this phase exists as a brittle phase within the material. The presence of this phase contributes to the inherent brittleness observed in traditional titanium alloys. In Ti_2AlNb alloy, this phase is relatively stable and does not undergo decomposition at lower temperatures. However, at higher temperatures, it may precipitate within the B2 phase or decompose into the O phase.

Table 1 Lattice parameters in the Ti_2AlNb alloy (Ref 2, 23)

Phase	Structure	Space group	Lattice constant, nm		
			a	b	c
α_2	hcp	$P6_3/mmc$	0.576	…	0.466
β	bcc	Im $\bar{3}$ m	0.331	…	…
B2	bcc	Pm $\bar{3}$ m	0.322	…	…
O1	ort	Cmcm	0.609	0.957	0.467
O2	ort	Cmcm	0.609	0.957	0.467

Compared to traditional titanium alloys, Ti_2AlNb alloy has gained significant attention from researchers due to the presence of the O phase. Since Banerjee's discovery of the O phase in 1988 (Ref 1), extensive research has been conducted on O-phase titanium alloys. The chemical composition of the O phase is Ti_2AlNb, and it adopts an ordered orthorhombic crystal structure with a space group of Cmcm, as shown in Fig. 5(c). Similar to the α_2 phase, the O phase also acts as a hardening phase within the alloy. The atomic occupancy relationships within the O phase have been theoretically studied by Wu et al. (Ref 23) Their research findings indicate that Ti atoms tend to occupy the α (8 g) sub-lattice, Al atoms tend to occupy the γ (4c1) sub-lattice, and Nb atoms tend to occupy the β (4c2) sub-lattice. The element content and types in the O phase are similar

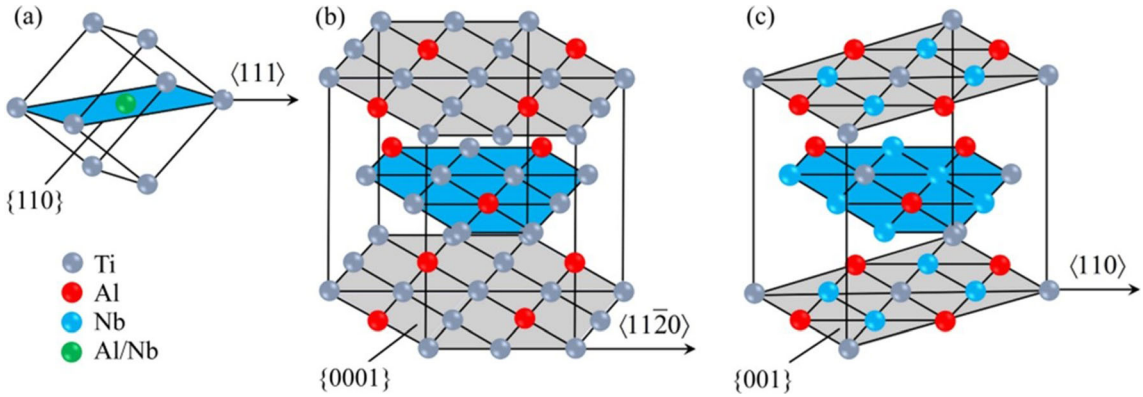

Fig. 5 Crystal structures of Ti-Al-Nb alloy (Ref 26): (a) B2 phase, (b) α_2 phase, and (c) O phase. Reprinted from M. Peters and C. Leyens, *Titanium and Titanium Alloys: Fundamentals and Applications,* John Wiley & Sons. Copyright © 2003 Wiley-VCH Verlag GmbH & Co. KGaA

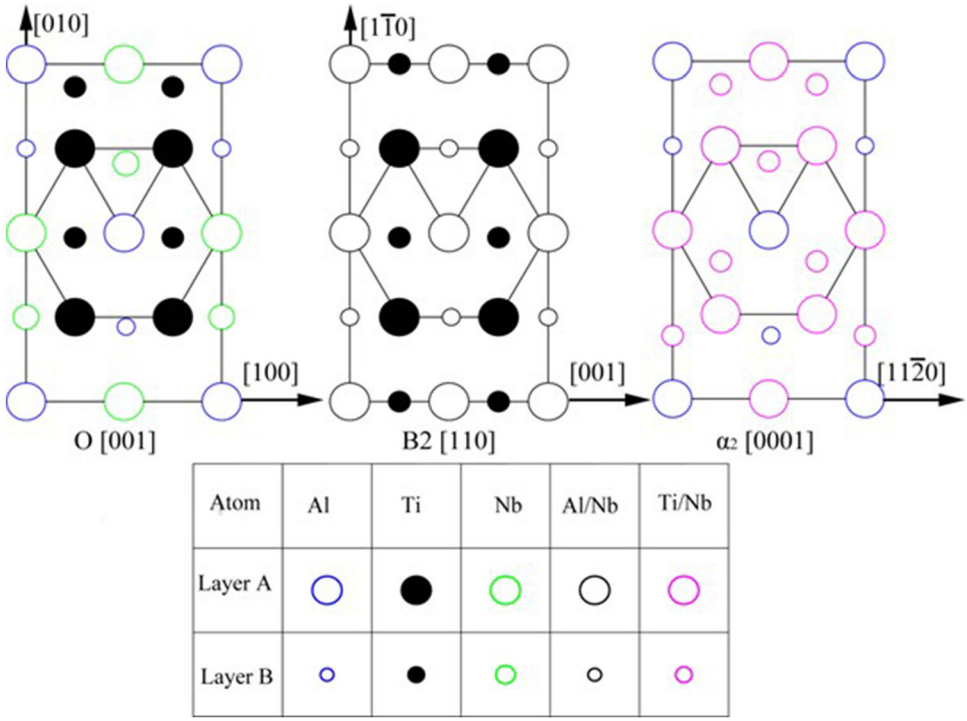

Fig. 6 Crystal lattices of O phase, B2 phase, and α_2 phases (Ref 27). Reprinted from *Progress in Materials Science,* Vol 42, D. Banerjee, The intermetallic Ti_2AlNb, Pages No. 135-158, Copyright 1997, with permission from Elsevier

to those in the B2 phase. The main difference between the O phase and the α_2 phase lies in the Nb element content. Ti_2AlNb alloy, with the presence of the O phase, exhibits outstanding creep resistance, good high-temperature stability, and remarkable strengthening effects compared to traditional B2 + α_2 phase titanium alloys (Ref 28). In comparison to the α_2 phase, the compatibility of crystal structure between the O phase and the B2 phase matrix is better. The substantial presence of the O phase mitigates the inherent brittleness caused by the α_2 phase, thereby enhancing the high-temperature stability of Ti_2AlNb alloy (Ref 29).

Figure 6 depicts the relationship between crystal structure and atomic occupancy of Ti_2AlNb alloy. This relationship was initially proposed by Muraleedharan et al. (Ref 30) The figure illustrates the mapping projection of the O phase along the [001] direction, the B2 phase along the [110] direction, and the α_2 phase along the [0001] direction.

4.2 a_2 Phase Formation Mechanism

In this alloy, there are two forms of the α_2 phase: equiaxed α_2 phase and lamellar α_2 phase. The precipitation of the α_2 phase is primarily associated with the matrix phase (B2 phase). In this alloy, a B2/β to α_2 phase transformation occurs during high-temperature cooling process. In the typical ideal scenario, different variants of the α_2 phase can occur within the material. Among them, the B2 phase has six $\{011\}_{B2}$ planes, and each plane has two $< 111 >_{B2}$ directions. Theoretically, there are a total of 12 variants of Burgers orientations in α_2 phase with

equal probabilities of occurrence (Ref 31), as shown in Table 2. In actual production processes, it is common for one or several α_2 textures to form, leading to a significant increase in the occurrence probability of these specific α_2 phase variants due to the selection effect (Ref 32-34). This means that certain α_2 variants are more likely to appear compared to other variants. At this point, the relationship between the texture and the matrix phase is illustrated in Fig. 7. Research findings indicate that this texture is primarily generated due to the combined effects of externally applied stress/strain and internal stresses. Additionally, the influencing factors of the selection effect extend beyond these factors and include the effects of dislocations, grain boundaries, and slip bands, among others.

4.3 O Phase Precipitation Mechanism

According to extensive research conducted by numerous investigators, the precipitation mechanisms of the O phase can be classified into three types: B2 $\rightarrow$ O, $\alpha_2 \rightarrow$ O, and B2 + $\alpha_2 \rightarrow$ O. Hereafter, a detailed description of each precipitation mechanism is provided as follows.

Table 2 Orientation variants of α_2 phase precipitation (Ref 35)

Variant number	Corresponding plane	Corresponding direction
1	$(0001)_{\alpha2}//(011)_{B2}$	$[2\ \bar{1}\bar{1}\ 0]_{\alpha2}//[\ \bar{1}\bar{1}\ 1]_{B2}$
2		$[2\ \bar{1}\bar{1}\ 0]_{\alpha2}//[1\ \bar{1}\ 1]_{B2}$
3	$(0001)_{\alpha2}//(\bar{1}\ 01)_{B2}$	$[2\ \bar{1}\bar{1}\ 0]_{\alpha2}//[1\ \bar{1}\ 1]_{B2}$
4		$[2\ \bar{1}\bar{1}\ 0]_{\alpha2}//[111]_{B2}$
5	$(0001)_{\alpha2}//(0\ \bar{1}\ 1)_{B2}$	$[2\ \bar{1}\bar{1}\ 0]_{\alpha2}//[111]_{B2}$
6		$[2\ \bar{1}\bar{1}\ 0]_{\alpha2}//[\ \bar{1}\ 11]_{B2}$
7	$(0001)_{\alpha2}//(101)_{B2}$	$[2\ \bar{1}\bar{1}\ 0]_{\alpha2}//[\ \bar{1}\ 11]_{B2}$
8		$[2\ \bar{1}\bar{1}\ 0]_{\alpha2}//[\ \bar{1}\bar{1}\ 1]_{B2}$
9	$(0001)\alpha2//(\bar{1}\ 10)_{B2}$	$[2\ \bar{1}\bar{1}\ 0]_{\alpha2}//[\ \bar{1}\bar{1}\ 1]_{B2}$
10		$[2\ \bar{1}\bar{1}\ 0]_{\alpha2}//[111]_{B2}$
11	$(0001)_{\alpha2}//(110)_{B2}$	$[2\ \bar{1}\bar{1}\ 0]_{\alpha2}//[1\ \bar{1}\ 1]_{B2}$
12		$[2\ \bar{1}\bar{1}\ 0]_{\alpha2}//[\ \bar{1}\ 11]_{B2}$

Type I: B2 $\rightarrow$ O. There are currently two different viewpoints regarding the precipitation mechanism of the O phase. Previous studies (Ref 36) demonstrated that the pseudotwins in the B2 phase form in the Ti-Al-Nb alloys. Analysis results show that all twins observed in the alloy belong to the intermediate metastable B19 phase. The first viewpoint of O phase precipitation mechanism suggests that under the influence of stress, the B2 phase undergoes shear displacement along the (111) [110] direction, leading to the formation of the B19 phase. Subsequently, the B19 phase further transforms through an ordering process to form the O phase (Ref 37). The process can be described as B2 $\rightarrow$ B19 $\rightarrow$ O. The presence of the B19 phase has been observed in the relevant process by Zhou et al. (Ref 37) and Bendersky et al. (Ref 38) using different techniques. The study conducted by SADI et al. (Ref 39) indicates that the transformation from the B2 phase to the O phase occurs through a phase transition process, where the B2 phase contracts along the a-axis and expands along the b-axis and c-axis to form the O phase. However, another viewpoint (Ref 40) suggests that the B2 phase directly undergoes a phase transition to form the O phase, without the presence of an intermediate phase.

Type II: $\alpha_2 \rightarrow$ O. Theoretically, there are six variants of Burgers orientations in the O phase that can precipitate within the α_2 phase (Ref 1). Similar to the precipitation of the O phase from the B2 phase, there are two different viewpoints regarding the precipitation of the O phase within the α_2 phase, both of which have experimental evidence. The first viewpoint suggests that the α_2 phase undergoes modulation decomposition. As the Nb content increases in the alloy, the Nb content within the α_2 phase also increases, resulting in Nb element oversaturation in this phase. The oversaturation of Nb atoms in the lattice destabilizes the crystal structure, leading to the migration of solute Nb atoms. This results in the formation of Nb-poor and Nb-rich regions within the phase. The Nb-rich regions exhibit significant lattice distortion and have an elemental composition closer to Ti_2AlNb, forming the O phase. The activation energy

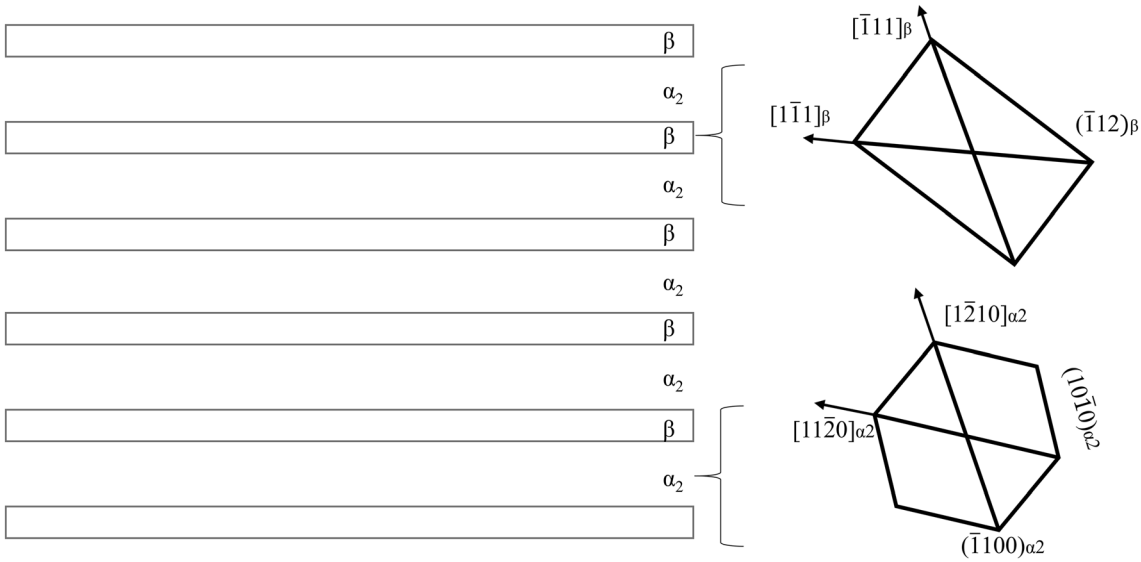

Fig. 7 Schematic diagram of Burgers orientation between B2/β and α_2 (Ref 26). Reprinted from M. Peters and C. Leyens, *Titanium and Titanium Alloys: Fundamentals and Applications,* John Wiley & Sons. Copyright © 2003 Wiley-VCH Verlag GmbH & Co. KGaA

for the lattice transformation in this case is the lattice distortion energy. Evidence supporting the modulation decomposition of the α_2 phase to generate the O phase has been provided by Wang et al. (Ref 40) and Huang et al. (Ref 41), who observed small O phase precipitates within the α_2 phase. Khadzhieva et al. (Ref 42) demonstrated through their research that stacking faults (SFs) exist within the primary α_2 phase, providing a site for Nb segregation and accumulation. The segregation of Nb atoms leads to significant lattice distortion in that region, and under the driving force of lattice distortion energy, the α_2 phase transforms into the O phase. A schematic representation of this phase transformation is shown in Fig. 8. The second viewpoint suggests that atomic ordering occurs within the α_2 phase, directly generating the O phase. Banerjee et al. (Ref 1) observed similar diffraction patterns for both phases, suggesting that the O phase is formed due to slight lattice distortion in the α_2 phase. Similarly, Wu et al. (Ref 43) found similar results, indicating similar crystal structures for both phases. The cylinder angles between the α_2 and O phases are reported to be 120° and 118°, respectively, indicating a small difference.

Type III: B2 + α_2 $\rightarrow$ O. The mechanism involves the co-precipitation of the O phase through a peritectic reaction between the B2 and α_2 phases, as illustrated in Fig. 9. The O phase can exist in various morphologies in Ti_2AlNb alloys, including lamellar, acicular-like, equiaxed, and ring forms. The formation mechanism of the ring O phase differs from that of other morphologies. Research conducted by Banerjee et al. (Ref 1) has demonstrated that the α_2 and B2 phases can undergo peritectoid reactions to generate the O phase. Subsequent studies (Ref 41) investigating the phase transformation behavior during heat treatment of the alloy revealed the presence of a light-colored phase surrounding the primary α_2 phase. Transmission electron microscopy (TEM) observations confirmed this phase to be the O phase. Therefore, under suitable heat treatment conditions, the O phase often forms around the periphery of the α_2 phase, and this particular state of the O phase is generated through the peritectoid reaction of B2 + α_2 $\rightarrow$ O (Ref 44).

4.4 Microstructure Characteristics

In general, Ti_2AlNb-based alloys exhibit multiple phases, microstructures, and phase composition in typical microstructures, as shown in Fig. 10. In this subsection, a detailed review is provided on the formation processes of these three types of typical microstructures.

The equiaxed structure is formed through spheroidization of the alloy, often achieved by subjecting it to thermal processing in the three-phase region (O + α_2 + B2). The equiaxed α_2 phase and O phase structure are derived from the B2 phase matrix, following a specific procedure: firstly, the alloy undergoes either solution treatment or aging treatment in the two-phase region (α_2 + B2), followed by quenching to preserve the high-temperature microstructure. Consequently, the heat-treated alloy develops equiaxed phases (O phase or α_2 phase) within the matrix (B2 phase) (Ref 45). Additionally, a ring-shaped O phase is observed surrounding the equiaxed α_2 phase in the initial microstructure of the alloy after isothermal forging (Ref 46). It can be observed that the α_2 phase can exist stably at lower temperatures and is less susceptible to decomposition during subsequent aging in the two-phase region (O + B2) (Ref 47, 48). Li et al. (Ref 49) investigated the phase transformation and microstructural evolution during aging of the alloy processed by spark plasma sintering and found that equiaxed O phase precipitation occurs at temperatures ranging from 700 to 850 °C. However, the microstructure containing equiaxed O and α_2 phases is relatively unstable at higher temperatures, rendering the alloy with equiaxed structure unsuitable for prolonged service at intermediate to high temperatures.

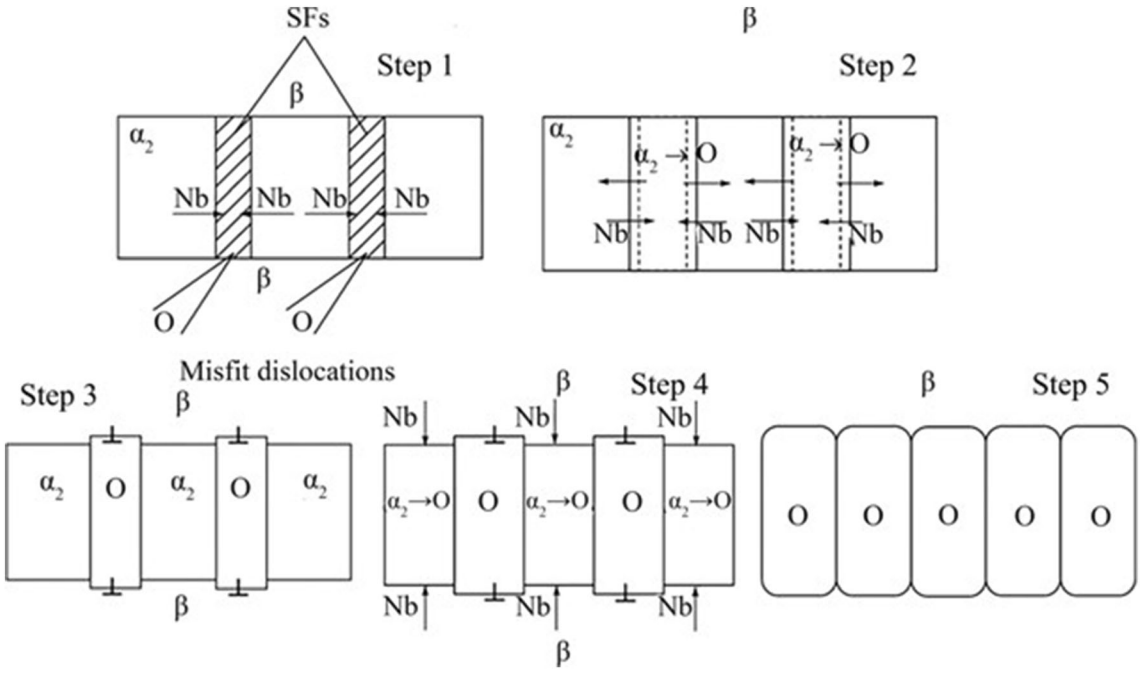

Fig. 8 Schematic diagram of phase transformation between O and α_2 (Ref 42). Reprinted with permission from O. G. Khadzhieva et al, Effect of aging on structure and properties of quenched alloy based on orthorhombic titanium aluminide Ti_2AlNb, *Physics of Metals and Metallography,* volume 115, pages 12-20, 2014, Springer Nature

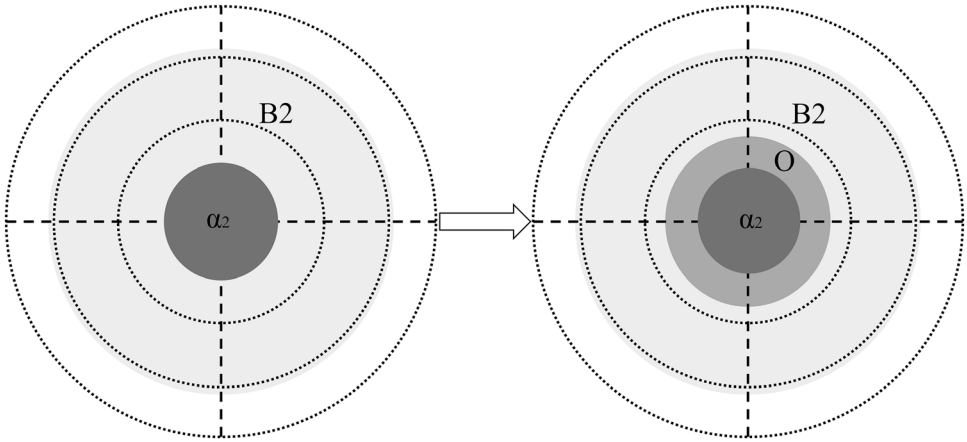

Fig. 9 Schematic diagram of peritectoid reaction between B2 and α_2. (The circles and axis are the scale-plate to show the phase dimension.)

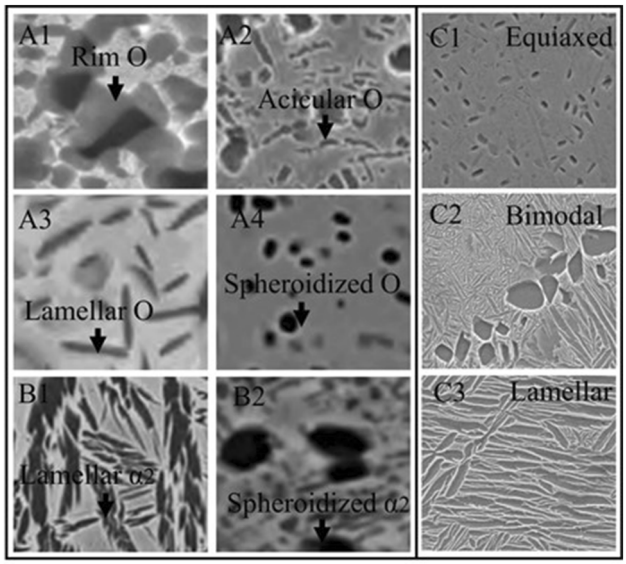

Microstructure	Phase composition
C1	A1, A4, B2
C2	A1, A2, A3, A4, B1, B2
C3	A2, A3, B1

Fig. 10 The typical phases, microstructures, and precipitated phase composition (B2 phase matrix) in typical microstructures of Ti_2AlNb alloy

The bimodal microstructure in the alloy can be considered as a combination of primary equiaxed or lamellar α_2 phase, O phase, O/B2 phase, and secondary Widmanstätten structures within the matrix. Achieving this type of microstructure requires a combination of suitable thermal processing and heat treatment. The equiaxed α_2 phase distributed along the grain boundaries is obtained by subjecting the alloy to solution treatment within the two-phase region (O + B2), with the solution treatment temperature being 20 °C lower than the β phase transformation temperature. The primary equiaxed α_2 phase thus formed impedes grain growth and prevents the presence of coarse grains that could have a significant impact on the material's mechanical properties. It has also been found that introducing small α_2 phase with a volume fraction of approximately 8 to 12% into the matrix is necessary to effectively suppress grain growth during heat treatment at temperatures close to the β phase transformation temperature.

In two-dimensional microstructural observations, the alloy's lamellar microstructures are often categorized as acicular-like, lamellar, and Widmanstätten structures (O phase or α_2 phase). The formation of lamellar O phase can be achieved by heating the alloy to a designated temperature range within the single-phase B2 region and then furnace-cooling to a lower temperature (< 600 °C). The thickness of the lamellar O phase is related to the cooling rate, where a lower cooling rate promotes an increase in the thickness of the lamellar O phase. Research by Hagiwara et al. (Ref 50) demonstrated that under such conditions, a semi-coherent relationship is maintained between the lamellar O phase and the B2 matrix. This semi-coherent relationship provides good compatibility between the two phases. When the cooling rate is low, coarse lamellar O phase and thicker intergranular α_2 phase can be observed in the material. However, this microstructure significantly compromises the material's mechanical properties.

Therefore, the formation of this morphology of the microstructure should be avoided as much as possible during thermodynamic processing and subsequent heat treatment. During aging in the O + B2 phase region, a considerable transformation of B2 phase to O phase occurs on the matrix, resulting in the direct precipitation of fine Widmanstätten structures. This precipitation hardening enhances the Vickers hardness (Range: 300-500 HV) and mechanical properties of the material during the aging process (Ref 51).

The material's properties mainly depend on the composition and morphological characteristics of the phases. The alloy with equiaxed phases exhibits good ductility at room temperature but has inferior high-temperature creep resistance and strength. On the contrary, the lamellar microstructures enhances the alloy's high-temperature creep resistance but reduces its room temperature ductility and toughness. The bimodal microstructure combines the advantages of both, achieving a balance between room temperature ductility, high-temperature creep resistance, and material strength. Therefore, determining the

optimal microstructure and phase morphology that enhance the material's mechanical properties and applying them in engineering applications has become an urgent issue.

4.5 Microstructure Regulation

The microstructure of Ti_2AlNb alloy is closely related to the types of processing techniques and heat treatment conditions. Not only in traditional material manufacturing processes such as forging, extrusion, and rolling, where the microstructure is influenced by deformation and heat treatment, but also in novel material manufacturing processes such as powder metallurgy and additive manufacturing, the microstructure is closely related to process parameters. In different processing techniques, the microstructure of Ti_2AlNb alloy can be significantly affected by controlling process parameters such as deformation amount, deformation rate, deformation temperature, and holding time. Proper process selection and optimization can achieve refinement, homogenization, and control of grain orientation in the alloy, thereby improving its performance. Furthermore, heat treatment conditions also play a crucial role in influencing the microstructure of Ti_2AlNb alloy. By controlling heat treatment parameters such as solution temperature, holding time, and cooling rate, the microstructural characteristics such as grain size, phase proportion, and phase morphology of the alloy can be adjusted. Appropriate heat treatment conditions can promote the formation of desired phase structures in the alloy and regulate the interactions between phases, thus enabling precise control over the alloy's performance. Therefore, a comprehensive understanding of the relationship between microstructure, processing techniques, and heat treatment conditions is of significant importance in advancing the development of Ti_2AlNb alloy in industrial applications. Such comprehensive understanding will help optimize the process flow, improve alloy performance, and drive the widespread application of this alloy in aerospace, automotive, and other fields.

Plastic deformation has an influence on the microstructural morphology. Temperature and crystal orientation affect the plastic deformation in alloy (Ref 52, 53). Thus, temperature and crystal orientation also affect the microstructural morphology in Ti_2AlNb alloy. In the case of Ti_2AlNb alloy, processes such as forging, extrusion, and rolling can cause fragmentation of the original microstructure. With increasing deformation, the lamellar structure is significantly fragmented, forming numerous spherical O-phase particles (Ref 54). Among various plastic processing methods, Boehkert et al. (Ref 55) suggested that multidirectional isothermal forging is a highly suitable process for this alloy. It effectively refines the as-cast microstructure, promotes homogenization of the microstructure, and provides sheet materials with a more uniform lamellar orientation. Zhang et al.'s research (Ref 56) indicates that the microstructure undergoes refinement after deformation of the alloy's grains. By employing sintering and extrusion processes to produce Ti_2AlNb alloy bars, during the extrusion process, the sintered alloy structure undergoes deformation, resulting in the disappearance of blocky α_2 phase and elongation of some B2 grains along the extrusion direction (Ref 57). Partial dynamic recrystallization occurs at the original B2 grain boundaries, leading to grain refinement and achieving the effect of fine grain strengthening.

Solution temperature has a significant impact on the microstructure of Ti_2AlNb alloy. According to the research by Zhou et al. (Ref 58), when solution is performed below the B2 single-phase region temperature (this temperature is about 1000 °C, and it is varied with elemental composition), the presence of α_2 phase at grain boundaries results in no significant change in the size of B2 grains, and their growth rate is slow. However, when solution is performed above the B2 single-phase region temperature, the α_2 phase at grain boundaries disappears, and the B2 grains rapidly grow, forming fully lamellar and larger-sized B2 grains. With increasing solution temperature, in order to reduce interfacial energy, the lamellar α_2 and O phases in the original microstructure gradually transform into equiaxed and coarsened morphology through atomic diffusion, with a decrease in proportion, while the proportion of the B2 phase gradually increases. Xue et al. (Ref 47) analyzed the influence of heat treatment on the microstructure of Ti-22Al-25Nb alloy and found that with increasing solution temperature, the small equiaxed O phases tend to coalesce or dissolve into the B2 matrix. Additionally, the solution temperature also has a significant effect on the precipitation of fine lamellar O phases during aging. At the same aging temperature, higher solution temperature leads to a higher proportion of fine lamellar O phase precipitation (Ref 59). The aging temperature effectively regulates the proportion of fine lamellar O phases. Moreover, when the solid solution temperature is fixed, the growth rate of B2 grains decreases with increasing solution holding time.

Aging temperature also affects the microstructure of Ti_2AlNb alloy. According to the research by Wang et al. (Ref 60), compared to the as-solution microstructure, with increasing aging temperature, the proportion of α_2 phase increases, the Rim-O phase surrounding the α_2 phase becomes thicker, and the α_2 grains embedded within the Rim-O phase completely dissolve, partially transforming into equiaxed O phase, which continues to grow. Fine lamellar O phase precipitates in the aged microstructure. The precipitation of O phase is highly sensitive to aging temperature. Under the same solution temperature, the secondary precipitation proportion of fine lamellar O phase decreases, its thickness increases, and its length decreases with the increase of aging temperature (Ref 61). However, the thickness of the primary coarse lamellar phase shows no significant influence with respect to aging temperature. However, aging treatment does not have a pronounced effect on the growth of B2 grains. Huang et al.'s research (Ref 62) discovered that when the alloy is subjected to aging treatment while in the α_2 + B2 two-phase region, the stability of the lamellar α_2 phase is not as previously reported. Spontaneous transformation of $\alpha_2 \rightarrow$ B2 + O phase occurs during annealing at 650 °C, and fine lamellar O phase layers form within the matrix.

Cooling rate is an important factor influencing the phase composition and phase proportions of the alloy. Research on the as-solution microstructure at different cooling rates has shown that water quenching results in an alloy consisting of continuous B2 phase and a small amount of residual O phase, while furnace cooling leads to the formation of numerous lamellar O phase lamellar and discontinuous B2 phase (Ref 63). It can be observed that at slower cooling rates, the microstructure has sufficient time for the transformation from β/B2 to O phase, and the lamellar O phase exhibits a greater thickness at lower cooling rates (Ref 64). Subsequently, during the aging process, more fine lamellar O phase layers precipitate.

Ti_2AlNb alloy exhibits static coarsening behavior during aging. In the initial stage of aging, significant coarsening occurs due to the Ostwald ripening mechanism (Ref 65) (refer to

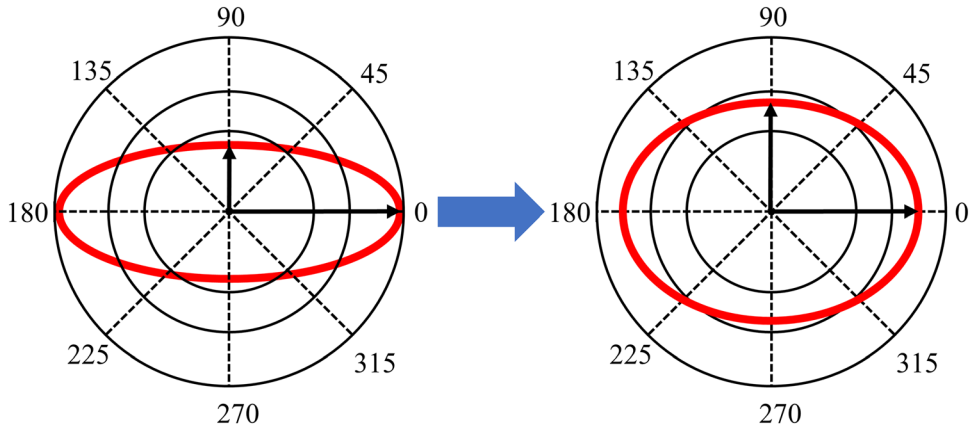

Fig. 11 Ostwald ripening mechanism. (The circles and axis are the scale-plate to show the phase dimension.)

Fig. 11). This mechanism elucidates the presence of size-disparate phases within the material, wherein the smaller phases dissolve and deposit onto the larger ones. The driving force behind this process stems from the energy disparity between larger and smaller structural entities. In accordance with thermodynamic principles, it is well-established that the surface energy of a given structure surpasses that of its interior. Consequently, the energy density of larger structures markedly falls short of that exhibited by smaller structures. This predilection facilitates the facile dissolution of smaller structural entities into the material matrix, followed by their subsequent adhesion to the periphery of larger structures, thereby diminishing the energy density of the latter. Subsequently, boundary segmentation and termination migration mechanisms begin to control the coarsening process. This is because the interface energy between the end faces of O phase layers differs from the long axis, resulting in diffusion of solute atoms and causing coarsening and segmentation of the O phase layers. With increasing aging time, the O phase layers continue to coarsen, and the interfaces between O and B2 phases become more pronounced, with coarsening rate increasing with the concentration of diffusing solute atoms. Furthermore, higher aging temperatures enhance the kinetic effects of O phase layer coarsening, consistent with the results of Xue et al.'s research (Ref 66). Higher temperatures provide a higher diffusion activation energy that accelerates the growth of O phase layers. At the same time, the thickness of O phase layers increases with increasing aging time. The growth process of O phase layers is driven by energy reduction and the equilibrium of B2 phase atom concentration. In the initial aging stage, the alloy possesses higher stored energy, providing the driving force for atomic diffusion and boundary diffusion. As the aging time extends, the driving force for alloy growth decreases, and the concentration gradient of alloy elements decreases, making it difficult for the O phase layers to continue coarsening.

The sintering parameters in powder metallurgy have a significant influence on the microstructure and mechanical properties of Ti_2AlNb alloy. Wang et al.'s research (Ref 67) demonstrated the use of a staged sintering process, where the alloy was initially treated under preliminary sintering conditions of 630 °C/20 MPa/1.0 h, followed by sintering at 950-1300 °C/35 MPa/1.0-2.5 h, and finally subjected to furnace cooling. The sintered Ti-22Al-25Nb alloy exhibited a low elongation of less than 5.09%, indicating poor room temperature ductility. However, under the sintering conditions of 1250 °C/1.5 h, the Ti-22Al-25Nb alloy showed excellent comprehensive performance at 650 °C, with a tensile strength of 620.53 MPa and an elongation of 7.44%. Wang et al. (Ref 68) pointed out in their study that using a holding temperature of 903 K for 60 min at a pressure of 20 MPa, followed by a subsequent increase to 1523 K at 30 MPa for 120 min, and finally furnace cooling, the powder metallurgy-prepared alloy exhibited a maximum elongation of 146% at 1313 K and a strain rate of 1.04×10^4 s^{-1}, with a tensile strength exceeding 85 MPa.

5. Fabrication and Machining Processes

Since the discovery of this alloy, numerous researchers have been dedicated to investigating its forming methods. As depicted in Fig. 12, the current forming methods employed for this alloy primarily encompass processes such as pressure forming, machining, cutting, welding, powder metallurgy, and additive manufacturing. Nevertheless, these forming methods are still in the research stage when applied to this particular alloy, with limited industrial utilization. Therefore, one of the key research focal points in this chapter is to provide an overview of the advantages, disadvantages, and research frontiers for each of these forming methods.

5.1 Casting

Although casting has become an important means of producing industrial products, the Ti_2AlNb alloy has not been widely used in production due to several unresolved key issues (Ref 4). The specific details describing these key issues are as follows:

1. During the casting process, there is a tendency for the segregation of multiple alloying elements within the alloy, such as Al and Nb. This results in uneven chemical composition and phase distribution across the cross-section of the castings.
2. The alloy is prone to porosity formation during the casting process.
3. Undesirable crystalline textures can easily develop during the casting process.
4. Coarse grains (Fig. 13), which is the key issue for the application of this material in industry, in millimeters of

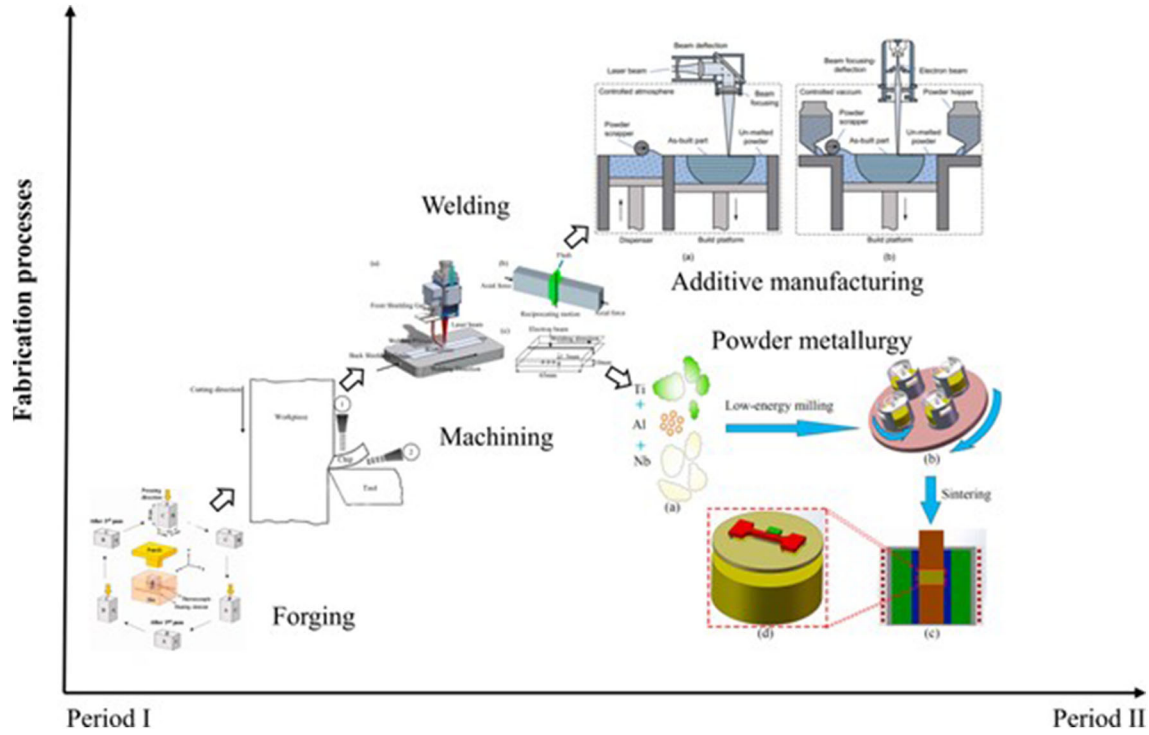

Fig. 12 The evolutionary progression of primary forming methods for this alloy

several types of Ti_2AlNb alloy, including Ti-22Al-23Nb, Ti-12Al-38Nb, Ti-23Al-27Nb, and Ti-25Al-25Nb, tend to form during the casting process.

The main reason for these issues lies in the significant differences in physical properties between the base material and the alloying elements, especially in terms of density and melting point (Ref 71). The aforementioned problems encountered during the casting process make it challenging to obtain high-quality deformable materials, semi-finished products, and welded structures. In particular, for the Ti_2AlNb alloy, due to its sensitivity to element composition and microstructure, its processability (plasticity, machinability, and weldability) as well as its mechanical properties (strength, ductility, and fracture toughness) are more complex compared to commercially available titanium alloys.

5.2 Forming under Pressure

In recent years, the issue of grain refinement in Ti_2AlNb alloy has become a key focus of research due to the presence of coarse grains. In the field of materials processing, it is typically achieved through thermoplastic deformation to increase dislocation density and promote the redistribution of dislocations, leading to dynamic recrystallization and subsequent grain refinement (Ref 28, 72). However, conventional plastic deformation techniques such as hot extrusion and hot rolling can only refine the grains of this alloy to a certain extent. To further refine the grain size, limitations arise from the achievable plastic deformation levels of traditional methods and the workability of the alloy, making the desired goals difficult to achieve. Consequently, in order to address these challenges, various methods of severe plastic deformation, such as high-pressure torsion (HPT), equal channel angular pressing (EACP), and multidirectional forging (MDF), have been widely adopted in the industrial sector (Ref 73, 74).

Through years of research, it has been discovered that multidirectional forging is the most suitable method for refining grain size in the Ti_2AlNb alloy, as illustrated in Fig. 14. Relevant studies (Ref 55) have indicated that multidirectional forging can refine the coarse grains produced during casting into fine-grained materials, as shown in Fig. 15(a) and (b), providing favorable billets for subsequent processing operations. Relevant researches, as shown in have demonstrated that multidirectional forging can refine the grains from centimeters to micrometer. Moreover, the alloy processed by multidirectional forging not only offers high-quality billets but can also be directly machined into components, such as turbine discs in aerospace engines. The desired microstructure can be achieved through the forging of the alloy after casting. As shown in Fig. 15(c) and (d), the alloy with lamellar microstructure can be transformed into bimodal microstructure with O phase spherization during plastic deformation. This phenomenon can be attributed to the morphology of lamellar O phase is easily affected by the heat and deformation.

Additionally, rolling can further optimize the mechanical properties of the material. Rolling is typically performed in the α_2 + B2 two-phase region or the α_2 + B2 + O three-phase region, aiming to refine the grains and strike a balance between toughness and strength. During the rolling process, key parameters such as coating methods, rolling speed, reduction rate, pass schedule, intermediate heat treatment temperature, and annealing temperature are focal points for researchers in the field of rolling technology (Ref 78). Studies have shown that rolling below the B2 single-phase region does not induce recrystallization and grain refinement; rather, as shown in Fig. 15(e) and (f), it elongates the grains along the rolling direction (Ref 79). Meanwhile, lamellar O phase can be

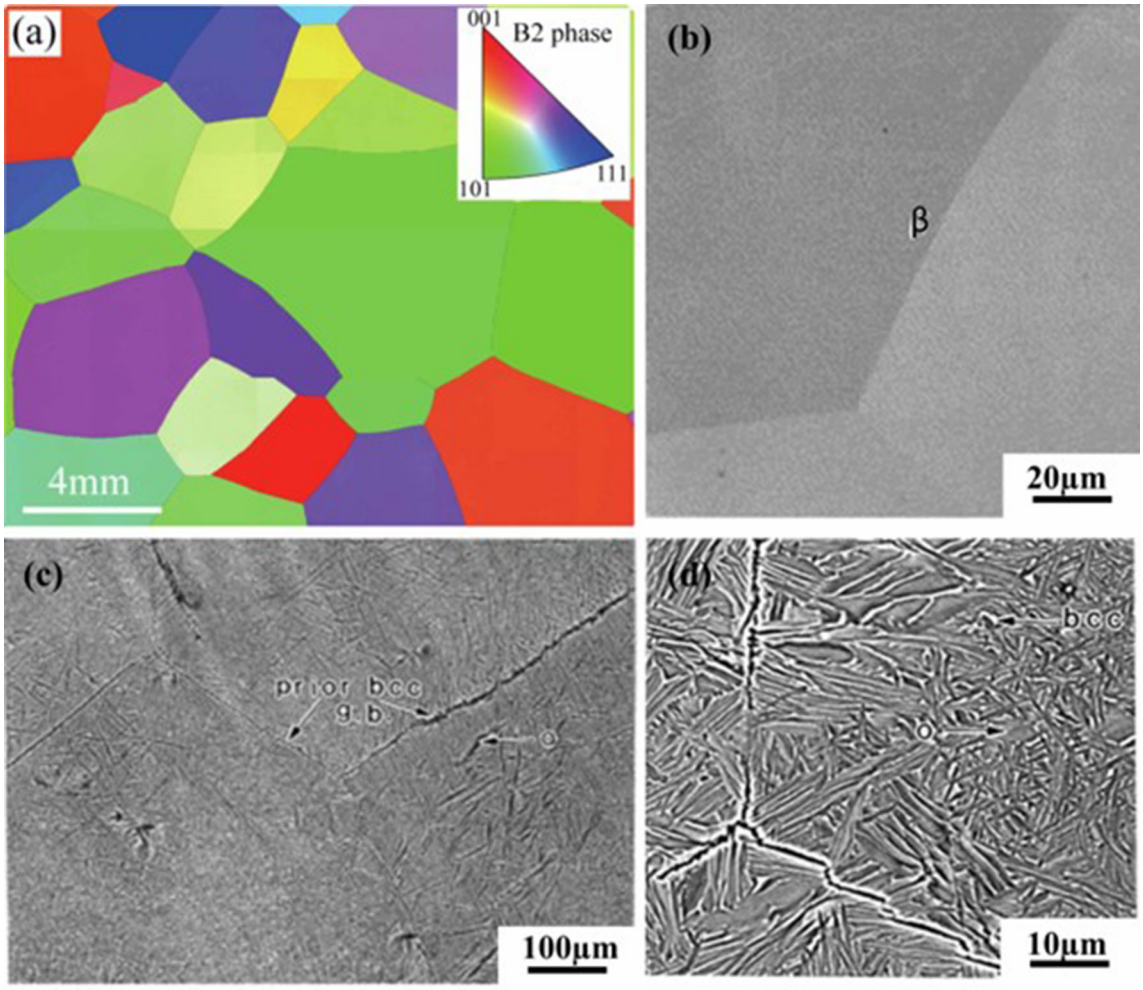

Fig. 13 Grain size of: (a) Ti-22Al-23Nb (Ref 69). (b) Ti-12Al-38Nb (Ref 70). (c) Ti-23Al-27Nb (Ref 70). (d) Ti-25Al-25Nb (Ref 70). (a) Reprinted from *Materials & Design,* Vol 225, Z. Yang, H. Liu, Z. Cui, H. Zhang, F. Chen, Refinement mechanism of centimeter-grade coarse grains in as-cast Ti_2AlNb-based alloy during multi-directional forging, Article No. 111508, Copyright 2023, with permission from Elsevier. (b)-(d) Reprinted from *Materials Science and Engineering: A,* Vol 279, C.J. Boehlert, The effects of forging and rolling on microstructure in O + BCC Ti Al Nb alloys, Pages No. 118-129, Copyright 2000, with permission from Elsevier

transformed into spheroidized O phase. Conversely, rolling within the B2 single-phase region promotes microstructural refinement (Ref 55). Investigations by Dey et al. (Ref 80) have emphasized the significant influence of rolling temperature and reduction on phase content, morphology, and texture evolution after rolling in both the B2 single-phase region and two-phase region. In the single-phase region, the alloy exhibits refined grains that meet the requirements when the reduction rate reaches 0.8. Conversely, other researchers (Ref 81) have achieved grain refinement by employing the pinning effect of hardening phases in the two-phase region, which involves a post-rolling aging treatment following high-temperature rolling. The aforementioned researches highlight that grain-refined materials processed through different techniques exhibit a favorable combination of room temperature plasticity and strength.

Overall, multidirectional forging has proven to be an effective method for refining the grain size in the Ti_2AlNb alloy. Subsequent rolling processes, whether conducted in the B2 single-phase region or the two-phase region (α_2 + B2 phases), can further enhance the material's mechanical properties. The comprehensive understanding of rolling parameters and their impact on phase content, morphology, and texture evolution is crucial for optimizing the rolling process (Ref 43). These findings contribute to the development of Ti_2AlNb alloys with fine-grained microstructures, enabling improved room temperature plasticity and strength, which holds significant promise for various applications in the field of materials science and engineering.

5.3 Machining

Due to the high specific strength and low thermal conductivity of Ti_2AlNb alloy at high temperatures, its machinability is poor (Ref 82). There are two main factors contributing to the poor machinability. Firstly, during the cutting process of this alloy, challenges arise from high cutting temperatures and severe tool wear. Under conventional cooling conditions, the tool surface temperature can reach up to 1000 °C when high-speed cutting this alloy (Ref 83). Such high temperatures pose significant challenges to cutting tools. As a result, the available types of tools for practical cutting processes are very limited. Previous studies have shown that the wear rate of carbide tools, polycrystalline diamond tools (PCD), and cubic boron nitride

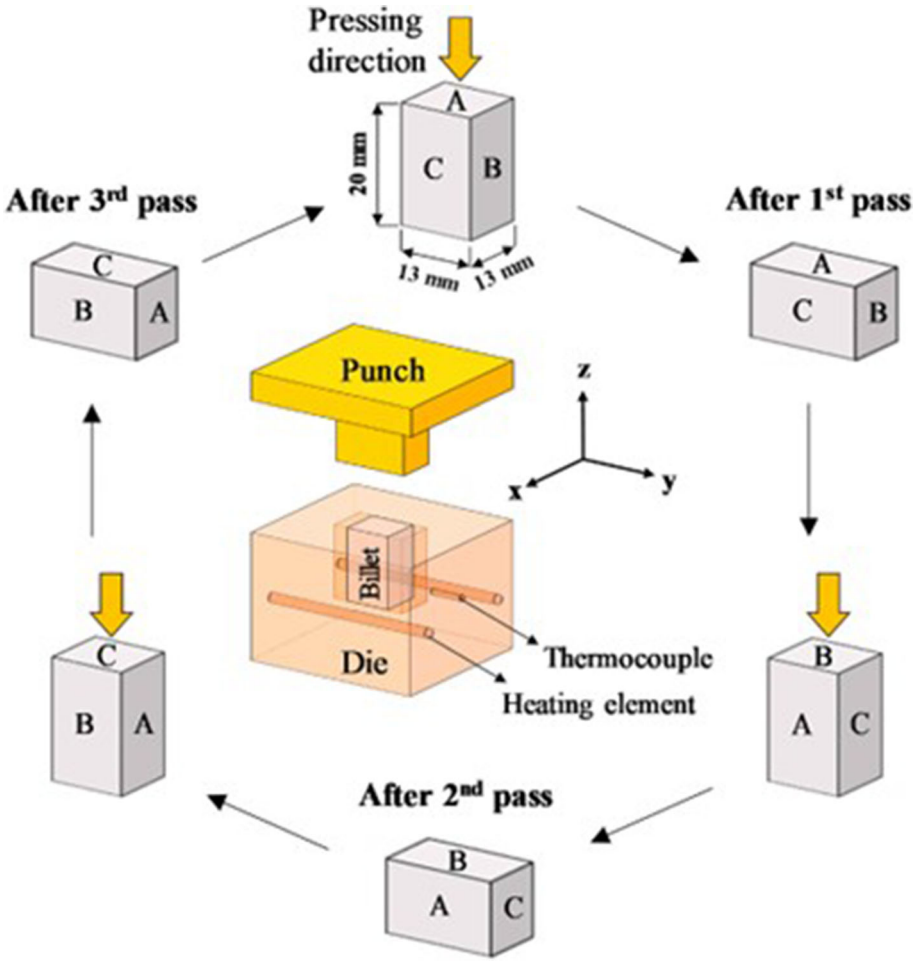

Fig. 14 Schematic diagram of multidirectional forging (Ref 75). Reprinted from *Materials Science and Engineering: A,* Vol 817, N. Azizi, R. Mahmudi, Microstructure, texture, and mechanical properties of the extruded and multi-directionally forged Mg-xGd alloys, Article No. 141385, Copyright 2021, with permission from Elsevier

tools (CBN) significantly accelerates when the temperature exceeds 740, 760, and 900 °C, respectively (Ref 84). Although some tools such as ceramic cutting tools (e.g., alumina matrix, Si3N4), super hard cutting tools (e.g., CBN, PCBN) can be used for processing this alloy, their high cost is discouraging. Therefore, it is essential to balance processing efficiency and cost when selecting machining methods. The second factor lies in the high affinity between titanium and aluminum atoms in Ti_2AlNb alloy and tool materials. The high cutting pressure during the cutting process firmly welds the workpiece to the tool surface. Consequently, part of the tool materials is torn or sheared and flies away with the chips, resulting in severe adhesive wear (Ref 85). Moreover, during high-temperature cutting processes, tool materials are more prone to oxidation reactions and diffusion phenomena, leading to significant oxidation fatigue and diffusion layers on the tool. Additionally, the strength and hardness of tool materials also decrease significantly with increasing cutting temperature, causing severe abrasive wear.

Cutting speed and cutting depth play a vital role in controlling the microstructure of Ti_2AlNb alloy, as shown in Fig. 16. The degree of chip segmentation correlates positively with cutting speed and cutting depth. The chip morphology of Ti_2AlNb alloy exhibits varying characteristics under different cutting conditions. As the cutting speed and cutting depth increases, as shown in Fig. 16(b)-(f), the chip morphology of Ti_2AlNb alloy transitions from a continuous chip with very small sawtooth features on the free surface to a serrated chip with adiabatic shear bands, consistent with the theory of thermoplastic instability. Additionally, deformation bands reveal elongated structures along the shear bands in the form of thin strips. Optimization of the combination of cutting speed and cutting depth can be employed to maintain continuous chip formation. To reduce tool wear during the cutting process, two main methods are currently employed. The first method involves developing more efficient tool materials and coatings that exhibit high chemical inertness with the workpiece materials while maintaining good mechanical properties at high temperatures.

The second method involves adopting more effective cooling technologies during machining, as illustrated in Fig. 17. The most commonly used method is conventional cooling, where coolant liquids are sprayed onto the machined surface and gradually infiltrate into the cutting zone. However, due to the extremely high temperature and high contact pressure on the tool surface, coolant liquids under conventional cooling conditions cannot effectively penetrate into the cutting zone, resulting in inadequate lubrication of the contact area and limited temperature reduction in the cutting area (Ref 86, 87). Fortunately, high-pressure jet cooling technology (HPJCT)

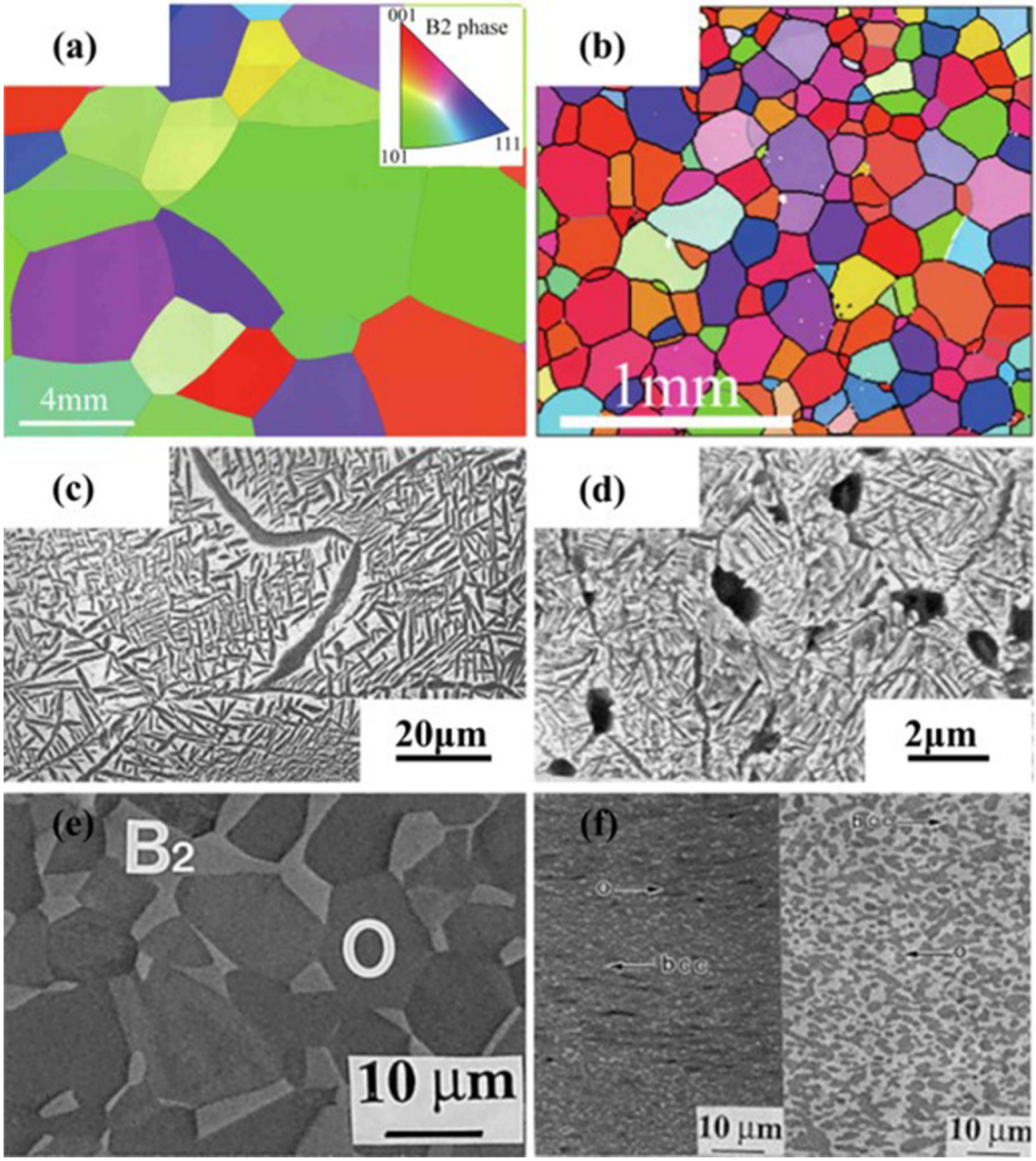

Fig. 15 Microstructure of Ti_2AlNb alloy: (a) before forging, (b) after forging (Ref 76); (c) before mechanical processing, (d) after mechanical processing (Ref 77); (e) before rolling, (f) after rolling (Ref 55). (a), (b) Reprinted from *Materials & Design,* Vol 225, Zhongyuan Yang, Haowei Liu, Zhenshan Cui, Haiming Zhang, Fei Chen, Refinement mechanism of centimeter-grade coarse grains in as-cast Ti_2AlNb-based alloy during multi-directional forging, Article No. 111508, Copyright 2023, with permission from Elsevier. (c), (d) Reprinted from *Materials Science and Engineering: A,* Vol 299, Jihua Peng, Yong Mao, Shiqiong Li, Xunfang Sun, Microstructure controlling by heat treatment and complex processing for Ti_2AlNb based alloys, Pages 75-80, Copyright 2001, with permission from Elsevier. (e), (f) Reprinted from *Materials Science and Engineering: A,* Vol 279, C.J. Boehlert, The effects of forging and rolling on microstructure in O + BCC Ti Al Nb alloys, Pages No. 118-129, Copyright 2000, with permission from Elsevier

provides an effective cooling solution by directly jetting coolant liquids into the cutting zone, dissipating a significant amount of heat and reducing frictional heat generation, thereby ultimately reducing the cutting temperature (Ref 88-90). Numerous studies (Ref 91-95) have demonstrated that high-pressure jet cooling technology not only significantly reduces tool wear and extends tool life but also improves chip breakability, machining efficiency, and surface integrity.

5.4 Welding and Joining

For the Ti_2AlNb alloy, the production of high-quality joint structures is crucial for its industrial applications. Currently, numerous researchers are developing various welding or joining processes to achieve high-quality joint structures. These emerging processes will expand the application range of the Ti_2AlNb alloy. Several welding methods, as shown in Fig. 18, have been investigated thus far to assess the welding perfor-

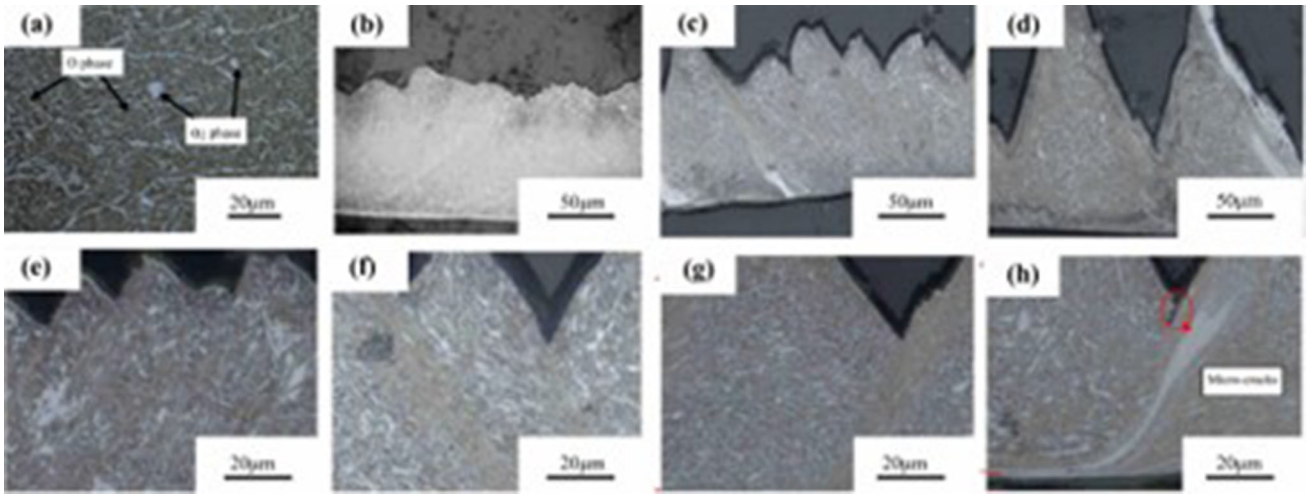

Fig. 16 Ti_2AlNb alloy: (a) Initial microstructure; the chip morphology under different cutting depth: (b) 0.06 mm, (b) 0.1 mm, and (c) 0.15 mm; the chip morphology under different cutting speeds: (e) 20 m/min, (f) 40 m/min, (g) 60 m/min, and (h) 80 m/min (Ref 83). Reprinted with permission from Linjiang He et al, Study on dynamic chip formation mechanisms of Ti_2AlNb intermetallic alloy, *The International Journal of Advanced Manufacturing Technology,* volume 92, pages 4415-4428, 2017, Springer Nature

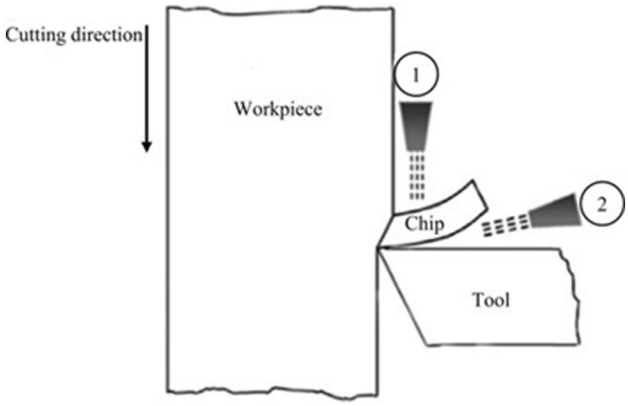

Fig. 17 Schematic diagram of the two types of coolant application: 1. Conventional coolant type, 2. High-jet pressure coolant type (Ref 82). Reproduced from International Journal of Lightweight Materials and Manufacture under the terms of the Creative Commons Attribution license

mance of the Ti_2AlNb alloy, including linear friction welding (Ref 96, 97), laser beam welding (LBW) (Ref 98-100), and electron beam welding (EBW) (Ref 101-103). Zou et al. (Ref 104) studied the microstructure and strength of joints in Ti-22Al-25Nb alloy during transient liquid phase diffusion bonding. The results indicated that appropriate holding time and high bonding temperature favor composition uniformity and interface bonding, resulting in robust joints. Quenching and tempering techniques can improve the microstructure and enhance the strength of the joints. Lei et al. (Ref 100, 105) studied the microstructural evolution and tensile properties of laser-welded Ti-22Al-27Nb and Ti-22Al-27Nb/TC4 joints, while Zhang et al. (Ref 99) investigated the laser weldability of dissimilar Ti-22Al-27Nb/TA15 alloy. As shown in Fig. 19(a) and (b), after laser welding of a Ti-22Al-25Nb alloy, the O phase in B2 matrix is disappeared. The laser-welded joints of this alloy exhibited low ductility at both room and high temperatures due to the columnar solidification structure formed in the weld and the precipitation of the O phase at the B2 grain boundaries. The influence of linear friction weld on microstructure is significant.

As shown in Fig. 19(c) and (d), prior to welding, the base metal exhibited a typical three-phase microstructure consisting of α_2, B2, and O phases. Specifically, the black granular phase and the grey acicular phase corresponded to the α_2 and O phases, respectively, while the matrix was predominantly B2 phase. Post-welding, the weld zone was primarily composed of B2 phase, with the granular α_2 phase and acicular O phase nearly disappearing. Chen et al. (Ref 96, 97) investigated the microstructural evolution and mechanical properties of linear friction welded Ti_2AlNb alloy under post-weld and post-weld heat treatment conditions. Solution and aging treatments significantly enhanced the microhardness in the welding zone, attributed to the precipitation hardening of the O phase and grain refinement strengthening. After aging treatment, the tensile strength of the joint further increased due to the secondary O phase precipitation, while the elongation decreased due to the suppression of the soft deformation mode in the fine needle-like microstructure. EBW is preferred for titanium alloy joining as it takes place in a clean vacuum chamber and offers high energy density and relatively low heat input (Ref 108, 109), resulting in narrow and deep penetrating welds, small heat-affected zones, low deformation, and residual stresses. Therefore, EBW has become the preferred method for welding Ti_2AlNb alloy.

As shown in Fig. 19(e) and (f), after electron beam welding, the equiaxed O and α2 phase appear in B2 phase matrix. Tan et al. (Ref 101-103) performed dissimilar welding of Ti-22Al-25Nb and TC11 alloys using EBW. In their study, heat treatments such as isothermal deformation and heat treatment were employed to improve the microstructure and mechanical properties of the welded joints.

It is worth noting that welded panel structures are widely applied in the aerospace industry. In practical applications, welding deformation has become a significant issue to be addressed due to the high requirements for structural integrity and dimensional accuracy. However, previous studies have mainly focused on the microstructure and mechanical properties of Ti_2AlNb alloy welding joints, with limited research on

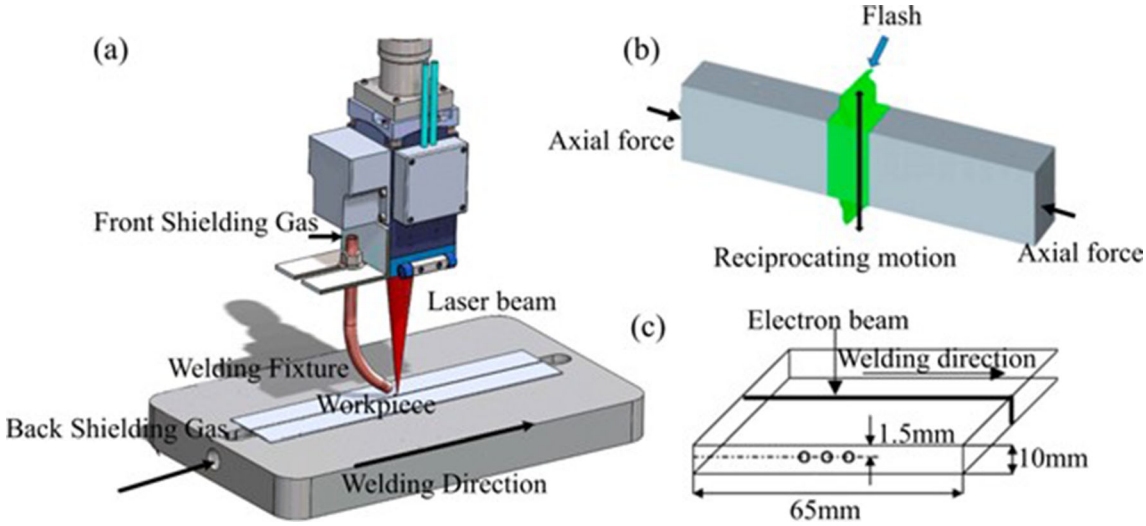

Fig. 18 Schematic diagram of (a) laser beam welding (Ref 98), (b) linear friction welding (Ref 97), and (c) electron beam welding (Ref 106). (a) Reprinted from *Journal of Alloys and Compounds,* Vol 681, Yanbin Chen, Kezhao Zhang, Xue Hu, Zhenglong Lei, Longchang Ni, Study on laser welding of a Ti-22Al-25Nb alloy: Microstructural evolution and high temperature brittle behavior, Pages No. 175-185, Copyright 2016, with permission from Elsevier. (b) Reprinted from *Materials Science and Engineering: A,* Vol 668, X. Chen, F.Q. Xie, T.J. Ma, W.Y. Li, X.Q. Wu, Microstructural evolution and mechanical properties of linear friction welded Ti_2AlNb joint during solution and aging treatment, Pages No. 125-136, Copyright 2016, with permission from Elsevier. (c) Reprinted from *Materials Science and Engineering: A,* Vol 392, Paolo Ferro, Andrea Zambon, Franco Bonollo, Investigation of electron-beam welding inwrought Inconel 706—experimental and numerical analysis, Pages No. 94-105, Copyright 2005, with permission from Elsevier

the influence of welding parameters on welding deformation. Therefore, investigating the deformation caused by welding of the Ti_2AlNb alloy is of great significance in promoting its application in aerospace structures.

5.5 Powder Metallurgy

During the production of Ti_2AlNb alloy products, traditional processing methods such as casting exhibit certain drawbacks, including issues of elemental segregation, grain coarsening, and shrinkage (Ref 110-112). These issues primarily arise from the differences in melting points, densities, and diffusion coefficients of the various elements present in the alloy (Ref 113). Research indicates that materials difficult to process using conventional methods can be effectively processed using powder metallurgy techniques (Ref 113), such as titanium-aluminum alloys, as shown in Fig. 20. Powder metallurgy techniques enable the retention of attractive physical properties of the material and facilitate the manufacturing of complex-shaped products, while offering advantages of simplicity, reduced processing time, and lower costs (Ref 114). The ability to manufacture complex-shaped products is particularly crucial for the production of challenging-to-form intermetallic compounds. Powder metallurgy processing, utilizing pre-alloyed titanium powders, has been demonstrated as a viable net-shaping technology. It has been proven to be a cost-effective method capable of producing complex structural components with performance comparable to those produced by traditional forging methods (Ref 67, 115, 116).

Within powder metallurgy techniques, blended elemental powder metallurgy (BEPM) offers economic advantages over pre-alloyed powder metallurgy, facilitating the alloying process (Ref 117). However, alloys synthesized using BEPM typically exhibit inferior mechanical properties, particularly in terms of ductility (Ref 118, 119). Extensive researches (Ref 120-123) have been conducted to understand the causes of low ductility. Research findings indicate that an increase in oxygen content resulting from powder metallurgy processes is the primary cause of reduced ductility. The elevated oxygen content promotes the formation of the brittle α_2 phase in Ti_2AlNb alloy, consequently decreasing the material's ductility. Recent research results (Ref 124-126) demonstrate that rare earth (RE) elements are highly effective in removing oxygen from titanium and titanium-aluminum alloys due to their superior chemical affinity for oxygen compared to titanium and aluminum elements. The addition of rare earth elements facilitates microstructure refinement, enhances the density of sintered compacts, and suppresses the precipitation of the brittle α_2/α phases in BEPM titanium alloys. Studies (Ref 127) have shown that the addition of 0.5 wt.% LaB6 can improve the elongation of pure titanium by 31.4%. However, pure rare earth metal powders are expensive and prone to oxidation, making them non-competitive. To overcome these obstacles, rare earth compounds are widely employed. Among various forms of rare earth, stable, easily grindable, and cost-effective LaB6 represents a potential choice. Additionally, the in-situ reaction between LaB6 and titanium or titanium-aluminum produces TiB short fibers, which are important strengthening phases and grain refiners in titanium and titanium-aluminum alloys (Ref 125, 127). Based on the aforementioned research findings, it can be inferred that the introduction of LaB6 holds promise for improving the performance of BEPM Ti_2AlNb alloys. However, there is currently limited research reported on the incorporation of LaB6 into the alloy.

In the production of powder metallurgy (PM) Ti_2AlNb-based alloys, efforts have been made, including the use of elemental powders (Ref 68) and pre-alloyed powders (Ref 128) through vacuum hot pressing sintering, as well as the utilization of pre-alloyed powders through hot isostatic pressing sintering (Ref 81, 114). However, the resulting microstructures from these sintering processes are typically found to be relatively

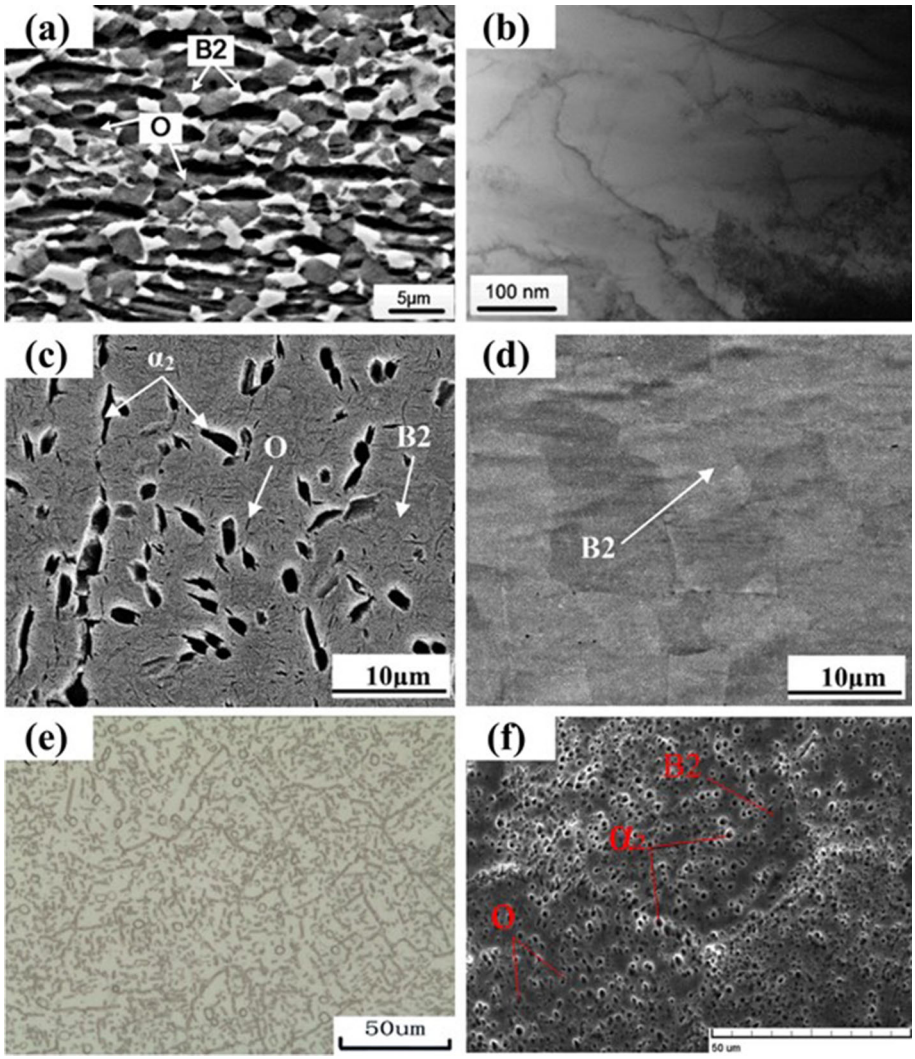

Fig. 19 Microstructure of (a) before laser beam welding, (b) after laser beam welding (Ref 98); (c) before linear friction welding, (d) after linear friction welding (Ref 107); and (e) before electron beam welding, (f) after electron beam welding (Ref 103). (a), (b) Reprinted from *Journal of Alloys and Compounds,* Vol 681, Yanbin Chen, Kezhao Zhang, Xue Hu, Zhenglong Lei, Longchang Ni, Study on laser welding of a Ti-22Al-25Nb alloy: Microstructural evolution and high temperature brittle behavior, Pages No. 175-185, Copyright 2016, with permission from Elsevier. (c), (d) Reprinted from Xiangqing Wu, Wenya Li, Tiejun Ma, et al, Oxidation Behavior of Three Different Zones of Linear Friction Welded Ti_2AlNb Alloy, *Advanced Engineering Materials,* John Wiley and Sons. © 2016 WILEY-VCH Verlag GmbH & Co. KGaA, Weinheim. (e), (f) These figures were published in *Aerospace Science and Technology,* Vol 14, L. Tan, Z. Yao, W. Zhou, H. Guo, Y. Zhao, Microstructure and properties of electron beam welded joint of Ti-22Al-25Nb/TC11, Page Nos. 302-306, Copyright Elsevier 2010

coarse, as sufficiently high sintering temperatures are required to fully consolidate these high-strength pre-alloyed powders. Spark plasma sintering (SPS) is a pressure-assisted pulsed electric current powder sintering technique that enables rapid heating, enhanced mass transfer, rapid consolidation, and near-net shaping concurrently. It has been proposed that the Joule heat generated by pulsed currents accelerates the densification of alloy powders by enhancing local plastic flow around connecting necks (Ref 129). It has been recognized that SPS is more effective in achieving microstructural homogenization compared to hot pressing sintering using mixtures of elemental and master alloy powders, as the intense Joule heating effect raises local temperatures, thereby increasing the diffusion rate. Niu et al. (Ref 110) conducted experimental investigations on the microstructure and mechanical properties of alloys after SPS and further optimized the microstructure through heat treatment, resulting in Ti_2AlNb-based alloy products with improved performance.

The microstructural changes of compacts prepared under different Hot Isostatic Pressing conditions are shown in Fig. 21. Low-temperature Hot Isostatic Pressing results in noticeable Prior Particle Boundaries (PPB), as illustrated in Fig. 21(a). As the temperature increases, inter-powder bonding improves but powder surface contours remain visible, as illustrated in Fig. 21(b). Further increasing the Hot Isostatic Pressing temperature eliminates powder surface contours, revealing a fine and uniform microstructure with grain sizes ranging from 30 to 50 μm, as shown in Fig. 21(c). This microstructure quality rivals that of materials produced by casting or forging but requires minimizing inherent gas pores in gas-atomized powders to ensure good mechanical properties.

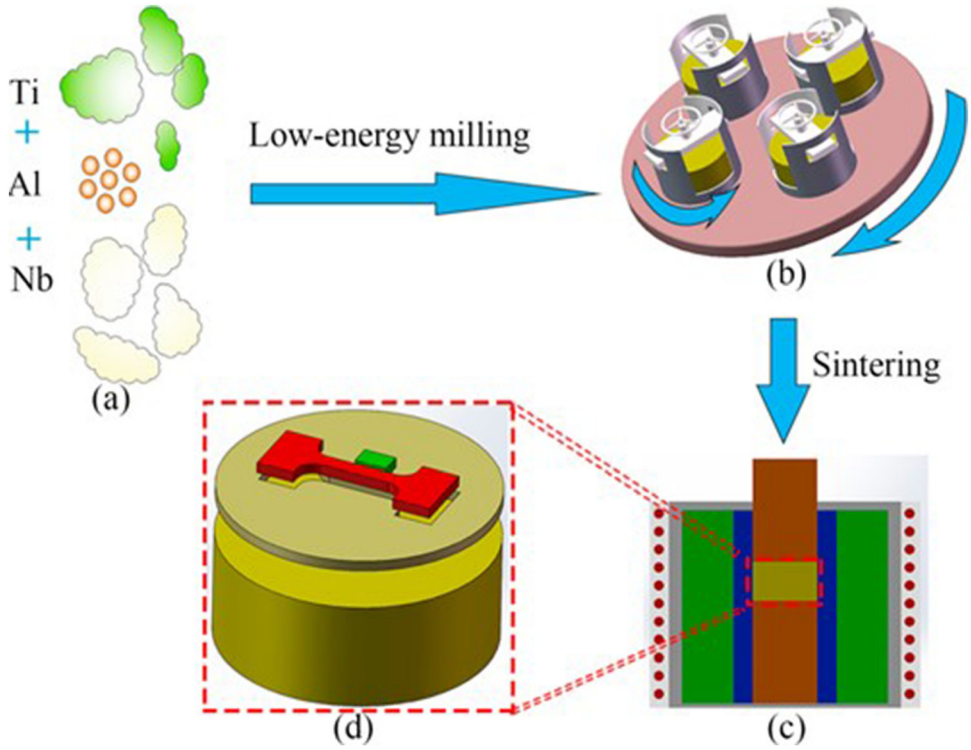

Fig. 20 Schematic diagram of powder metallurgy (Ref 67): (a) the blended powder, (b) the low-energy milling, (c) the sintering process, and (d) the sintered alloy. Reprinted from *Materials Science and Engineering: A,* Vol 654, Guofeng Wang, Jianlei Yang, Xueyan Jiao, Microstructure and mechanical properties of Ti-22Al-25Nb alloy fabricated by elemental powder metallurgy, Pages No. 69-76, Copyright 2016, with permission from Elsevier

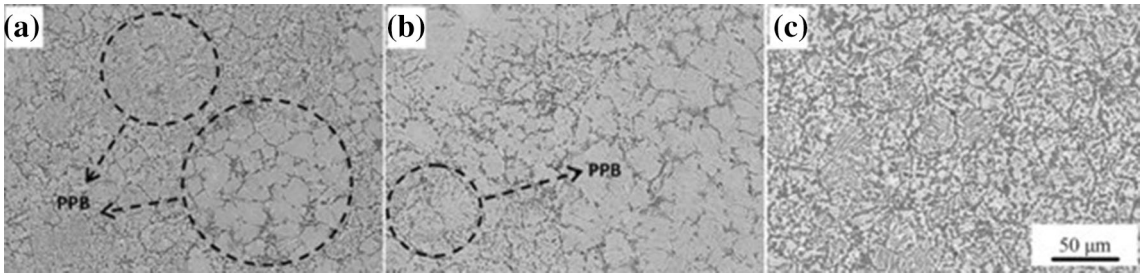

Fig. 21 Microstructures of powder metallurgy (Ref 130) prepared by hot isostatic pressing: (a) 980 °C/140 MPa/3 h, (b) 1010 °C/140 MPa/3 h, (c) 1030 °C/140 MPa/3 h. Reprinted from *Journal of Materials Science & Technology,* Vol 31, Jie Wu, Lei Xu, Zhengguan Lu, Bin Lu, Yuyou Cui, Rui Yang, Microstructure Design and Heat Response of Powder Metallurgy Ti_2AlNb Alloys, Pages No. 1251-1257, Copyright 2015, with permission from Elsevier

5.6 Additive Manufacturing

In the past three decades, the emergence of Metal Additive Manufacturing (MAM) technology has drawn attention from scientists and engineers towards the production applications of alloy (Ref 4). Currently, commonly used MAM techniques for this alloy include Powder Bed Fusion (PBF) (Ref 131, 132) and Directed Energy Deposition (DED) (Ref 4), as shown in Fig. 22.

As shown in Fig. 23(a)-(e), the observation reveals significant differences in microstructure between the bottom and top regions of the sample, primarily influenced by temperature variations during the Powder Bed Fusion process, particularly affected by platform preheating and laser heating cycles. The microstructure in the top region (Fig. 23b and c) displays a different morphology, presenting as elongated B2 + O lamellar structure, containing more O (Ti_2AlNb) phase precipitates compared to the bottom, likely due to lower processing temperatures. Additionally, microcracks observed in the top region suggest lower preheating temperatures compared to the bottom part.

The microstructure in the bottom region (Fig. 23d and e) exhibits a B2 + O + α2 structure with relatively coarse B2 grains. Under high magnification, elongated B2 + O microstructure is observed, with coarse α_2 (Ti3Al) phase precipitates along the boundaries of B2 grains, indicating aging of the alloy during the SLM process. Prolonged manufacturing times and high temperatures lead to B2 phase decomposition and α_2 phase precipitation in the bottom region. The experiments emphasize that titanium intermetallic alloys processed via Powder Bed Fusion under high-temperature platform preheating and laser heating cycles result in non-uniform

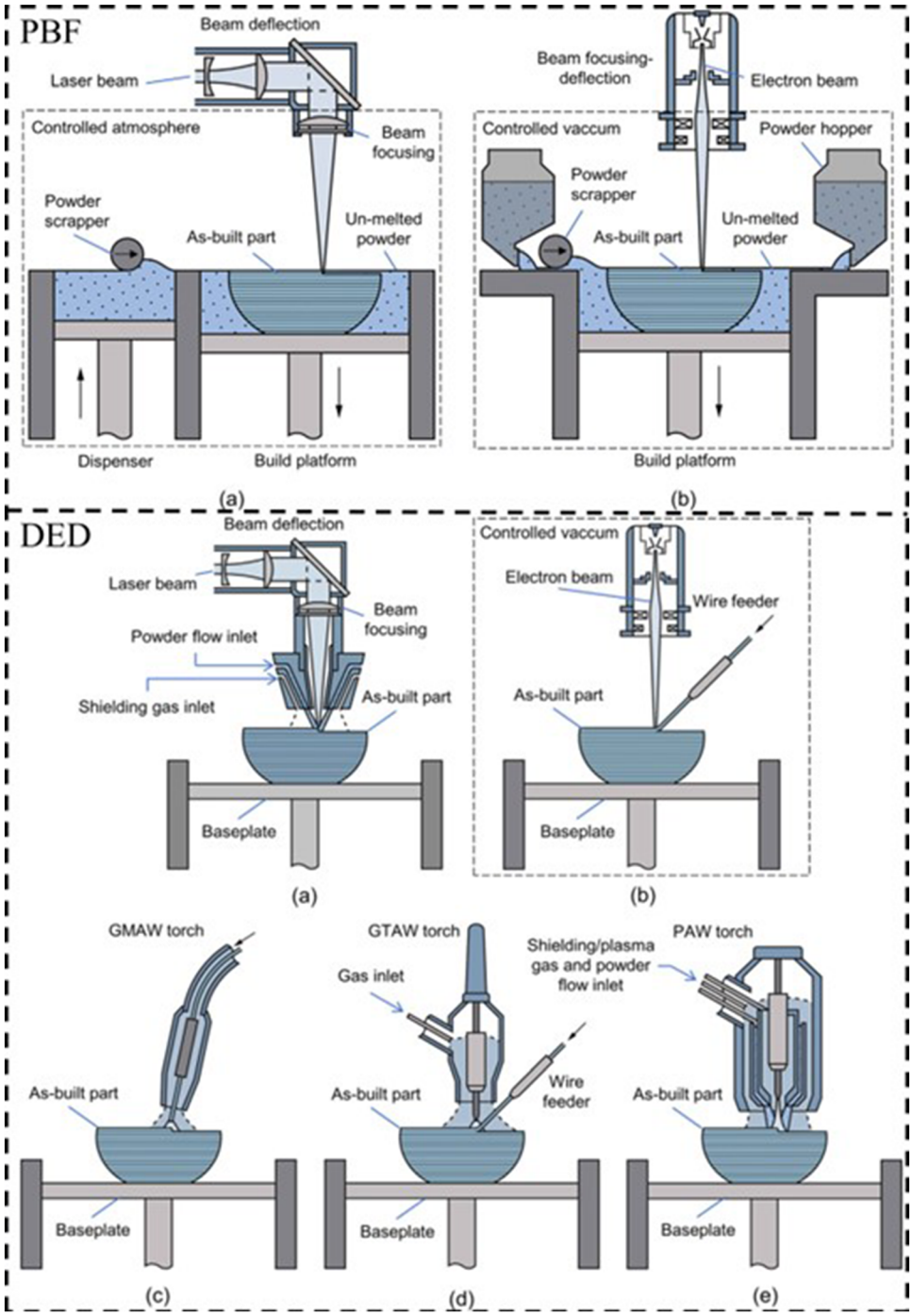

Fig. 22 Schematic diagram of Additive Manufacturing (Ref 133): Powder Bed Fusion (a) Laser power bed fusion, (b) Electron beam powder bed fusion; Directed Energy Deposition (a) Laser direct energy deposition, (b) Electron beam direct energy deposition, (c) Gas metal arc direct energy deposition, (d) Gas tungsten arc direct energy deposition, and (e) Plasma arc direct energy deposition. Reprinted from *Advances Industrial Manufacturing Engineering,* Vol 2, J.P.M. Pragana, R.F.V. Sampaio, I.M.F. Bragança, C.M.A. Silva, P.A.F. Martins, Hybrid metal additive manufacturing: A state-of-the-art review, Article No. 100032, Copyright 2021, with permission from Elsevier

microstructures along the build direction. This highlights the importance of controlling and optimizing processing parameters to achieve desired material properties and structural integrity. As shown in Fig. 23(f) and (g), the microstructure commonly observed in O-phase alloys produced by Directed Energy Deposition consists of B2/β-grains containing varying fractions of grain boundary O- or α2-precipitates, along with intragranular precipitates of lamellar O-phase. Plate-like colonies primarily grow from the boundaries or manifest as individual small O-platelets situated between these colonies. The current achievements and challenges of this technology can be summarized as follows: Firstly, MAM enables the production of dense, fine-grained materials with excellent mechanical performance combinations at room temperature, although they are not yet thermodynamically equilibrium in their initial state. Secondly, post-processing methods that can provide thermally

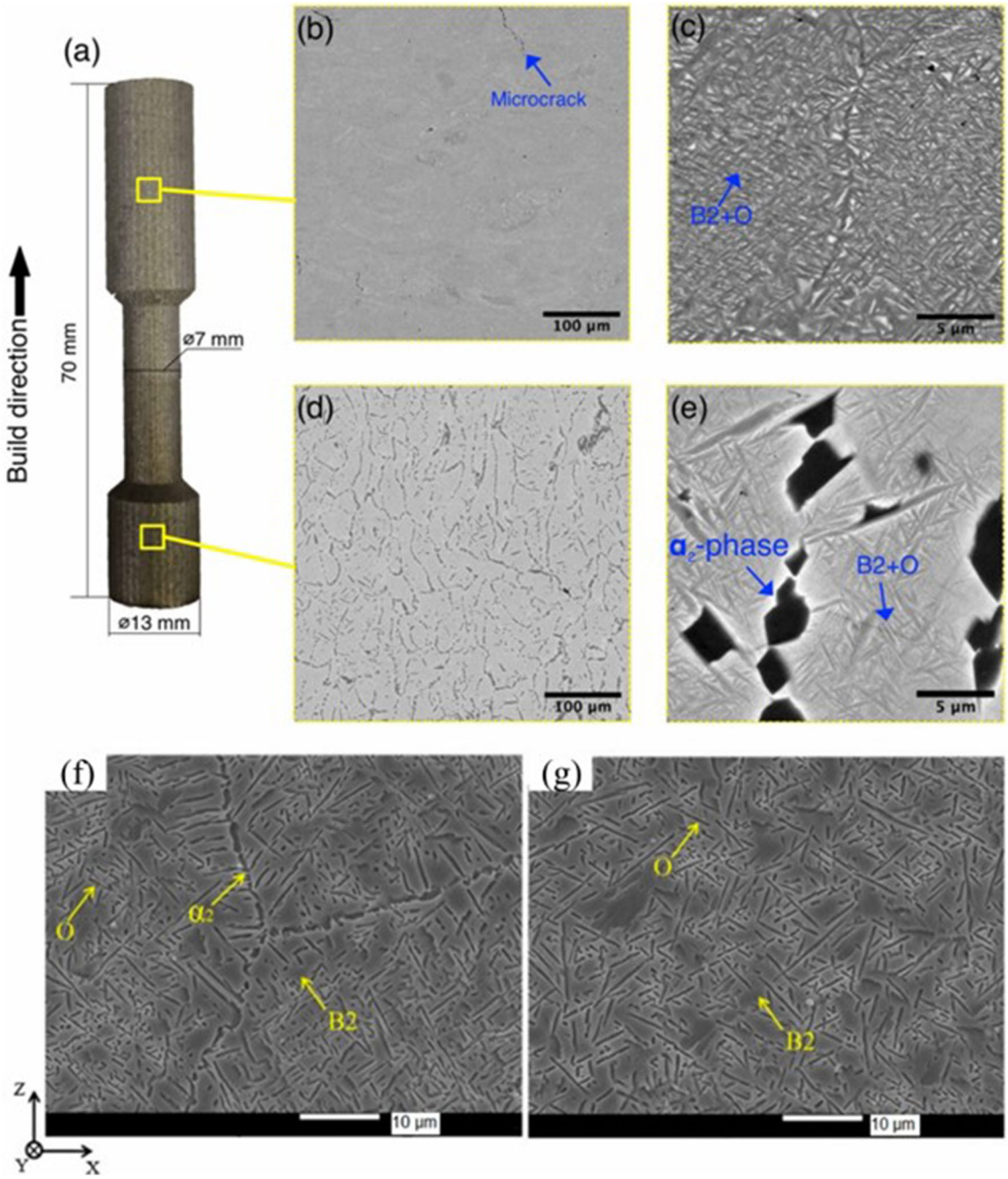

Fig. 23 (a) The tensile specimen built by Powder Bed Fusion (Ref 134), (b-c) the microstructure on the top of tensile specimen, (d-e) the microstructure on the bottom of tensile specimen; the microstructure of Directed Energy Deposition (Ref 4) (f) with grain boundary, and (g) without grain boundary. Reprinted from Materials under the terms of the Creative Commons Attribution license

stable structures and balanced properties at both room and high temperatures are yet to be developed. Thirdly, the dual-wire feeding method holds significant potential in the WAAM (Wire arc additive manufacturing) process for O-phase alloys. Fourthly, L-PBF (Laser-PBF) demonstrates exceptional mechanical properties for powder feedstock, while hybrid additive manufacturing processes combining L-DED (Laser-Directed Energy Deposition) and point forging exhibit promising results. Lastly, inkjet binding processes may not be the optimal choice for creating O-phase alloy structural parts due to increased porosity and longer post-processing time.

Future research can focus on detailed investigations of the effects of post-processing and chemical composition on the microstructure and mechanical properties, including cyclic loading, fracture toughness, and creep testing. This will ensure the development of heat treatment methods that provide a

performance combination comparable to refractory nickel, titanium, and titanium gamma-aluminide compounds within the operating temperature range of 600-700 °C.

5.7 Surface Treatment

For Ti_2AlNb alloy, low wear resistance poses a significant challenge in the fabrication of tribological components such as shafts and blades in gas turbines, engine valves, and turbochargers (Ref 135, 136). Surface modification is an effective and economical method to improve their tribological performance. The dual glow plasma surface alloying process known as the Korf Process has been proven to enhance the surface properties of metals or alloys, including microhardness, wear resistance, and oxidation resistance (Ref 137).

Previous studies have shown that a plasma surface chromizing layer on Ti_2AlNb alloy significantly improves its oxidation resistance at both room and high temperatures (Ref 138). Tungsten is a major component of commercially available hard alloys used for coating applications (Ref 139). As indicated in reference (Ref 140), tungsten occupies positions in the titanium sublattice, leading to changes in the electronic structure. Based on empirical electron theory, it is expected that tungsten occupying the titanium sublattice will primarily form a titanium-tungsten phase in the titanium-aluminum-niobium system. Research has revealed that the addition of tungsten to Ti_2AlNb-based alloys can enhance the wear resistance of the base material. Carbon, with its smaller atomic size, can diffuse deeply and form a WxC1-x/C coating, interacting with tungsten to create a W-C phase. This coating is chosen due to its low friction characteristics, higher relative hardness, and low surface energy, which are expected to reduce adhesion and wear (Ref 141). Relevant studies propose the method of plasma surface W-C dual-layer treatment. Figure 24 illustrates the microstructure of an Al/Cr coating on Ti_2AlNb alloy. Scanning electron microscopy (SEM) images reveal that the deposition of Cr (Fig. 24a) and Al (Fig. 24b) is uniform and dense, exhibiting no pores or cracks. At higher magnification, the Cr film appears polycrystalline with an island growth mechanism, while the Al crystals exhibit a layered growth mechanism. Cross-sectional morphology of the Al/Cr protective coating (Fig. 24c) and energy-dispersive x-ray spectroscopy (EDS) analysis (Fig. 24d) indicate that the coating surface consists of a dense Al layer (as seen in Fig. 24b), beneath which an Al-Cr alloy layer forms. This formation is primarily attributed to mutual diffusion between the Al and Cr layers during heat treatment, consistent with diffusion laws. Additionally, the presence of the Cr and diffusion layers results from the characteristics of double glow treatment, where Cr atoms sputter onto the substrate to form both a deposited layer and a diffusion layer at elevated temperatures. The diffusion within the Al/Cr coating enhances the bond strength between the coating and substrate, preventing delamination. The thickness of the Al/Cr coating measures 63 μm, as depicted in Fig. 24(d). Clearly, a diffusion zone has developed due to mutual diffusion between Cr, the substrate, and Al.

6. Mechanical Properties of Ti_2AlNb Alloy

Ti_2AlNb alloy, as an important structural material in the aerospace field, is evaluated based on its mechanical properties, which are closely related to its microstructural features. A thorough understanding of the relationship between tensile performance, fracture toughness, creep resistance, fatigue

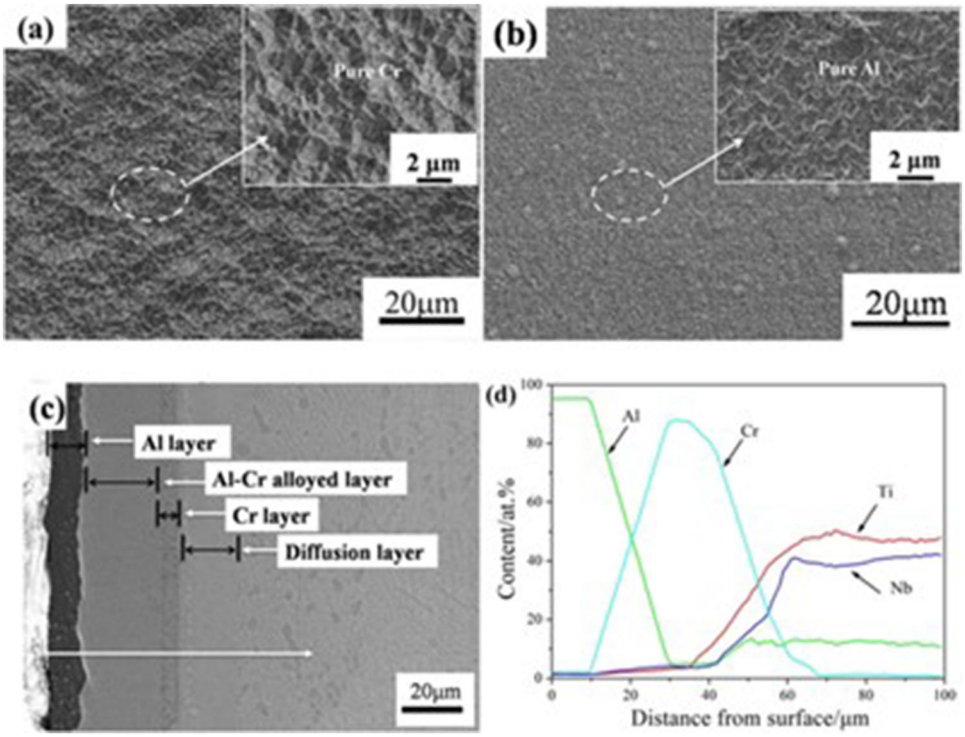

Fig. 24 SEM images of Al/Cr coating on Ti_2AlNb alloy (Ref 135) (a) Cr deposition, (b) Al deposition, (c) cross-section images (d) EDS result. Reprinted from *Materials Science and Engineering: A*, N. Azizi and R. Mahmudi, Microstructure, texture, and mechanical properties of the extruded and multi-directionally forged Mg–xGd alloy, Article No. 141385, Copyright 2000, with permission from Elsevier

Table 3 Physical parameters of advanced high temperature materials

Material	ρ, g cm^{-3}	Elasticity modulus, GPa	Yield strength, MPa	Tensile strength, MPa	RT ductility%	HT ductility%	Limit tem. of creep res., °C	Antioxidation limit tem., °C
Titanium	4.5	95-115	380-1150	480-1200	10-25	12-50	600	600
Ni-based	7.9-8.5	206	800-1200	1250-1450	3-25	20-80	800-1090	870-1090
γ-TiAl	3.7-4.2	160-180	350-600	500-800	1-4	10-60	750-800	800-900
Ti_2AlNb	5.3-5.7	110-145	900-1130	1010-1250	3-16	15-35	650-750	650-750

RT: Room temperature; HT: High temperature; tem.: temperature; res.: resistance

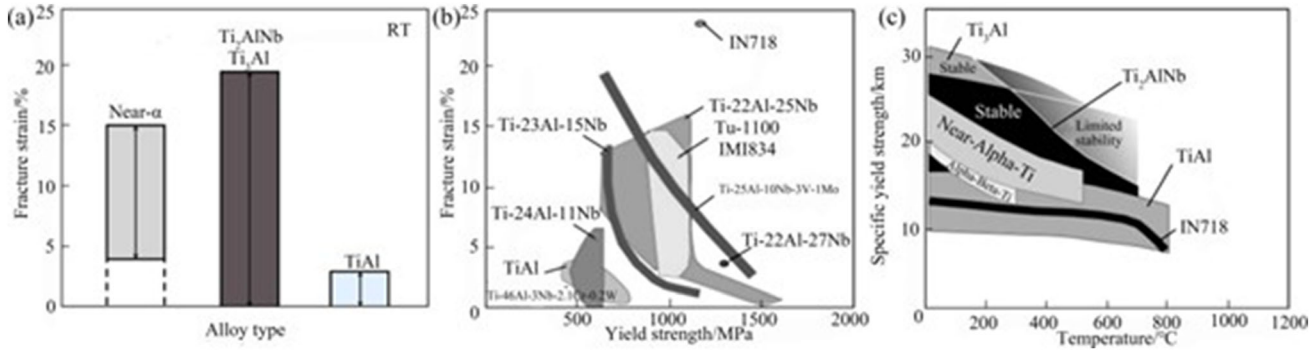

Fig. 25 Comparison of tensile properties and specific yield strength of Ti_2AlNb alloy and to near-α titanium, Ti_3Al, IN718 and TiAl alloy (Ref 26): (a) Fracture strain, (b) Fracture strain vs. yield strength, and (c) Specific yield strength. Reprinted from M. Peters and C. Leyens, *Titanium and Titanium Alloys: Fundamentals and Applications,* John Wiley & Sons. Copyright © 2003 Wiley-VCH Verlag GmbH & Co. KGaA

Table 4 Tensile properties of Ti_2AlNb alloy at room temperature

Nominal component	Deformed state	Microstructure	R_m, MPa	$R_{p0.2}$, MPa	A, %
Ti-12Al-38Nb (Ref 146)	Forge and roll	Lamellar	869	809	12.3
Ti-22Al-24Nb (Ref 146)	Forge and roll	Lamellar	916	836	4.5
Ti-22Al-25Nb (Ref 55)	Free forge	Duplex	1180	1100	3.5
Ti-22Al-27Nb (Ref 143)	Roll	Duplex	1160	1050	10.1
Ti-23Al-17Nb (Ref 147)	Forge	Duplex	1095	910	13.0
Ti-25Al-24Nb (Ref 146)	Forge and roll	Equiaxed	1237	1125	5.0
Ti-22Al-24Nb-3Ta (Ref 13)	Roll	Duplex	1110	1100	14
Ti-22Al-20Nb-7Ta (Ref 143)	Roll	Duplex	1320	1200	9.8
Ti-22Al-24Nb-2 V (Ref 13)	Roll	Lamellar	888	740	3.3
Ti-22Al-24Nb-2W (Ref 13)	Forge	Lamellar	960	860	0.8

R_m: Ultimate tensile strength; $R_{p0.2}$: yield strength; *A*: elongation.

performance, and microstructure is crucial for the future development of this alloy. Table 3 presents the differences in physical and mechanical properties between Ti_2AlNb alloy, nickel-based superalloys, and γ-TiAl alloys. From Table 3 and Fig. 25, it can be observed that there are no apparent defects in this alloy.

As shown in Table 4, the tensile performance of this alloy is influenced by factors such as alloy composition, microstructural state (phase types, proportions, phase, and grain sizes, etc.), heat treatment processes (solution treatment and aging temperature, time, and cooling rate after heat treatment), and deformation processes (forging, extrusion, and rolling, etc.). Zhang et al. (Ref 142) investigated the tensile performance of Ti-22Al-25Nb and Ti-22Al-23.9Nb-1.1Mo alloys. The addition of Mo element reduced the room temperature strength and plasticity but increased the high-temperature strength and plasticity due to the refinement of grain size caused by Mo addition. The addition of other alloying elements also affects the mechanical properties of the material, which requires further research. Tensile performance is closely related to the microstructural features. Li et al. (Ref 143) studied the relationship between microstructure and properties and found that a dual-phase microstructure exhibited a good balance between strength and plasticity. Fu et al. (Ref 144) investigated the influence of lamellar O phase on the mechanical properties of the alloy and found that the size and distribution state of the O phase affected the macroscopic mechanical response of the alloy. Additionally, Fu et al.'s study (Ref 145) revealed that the

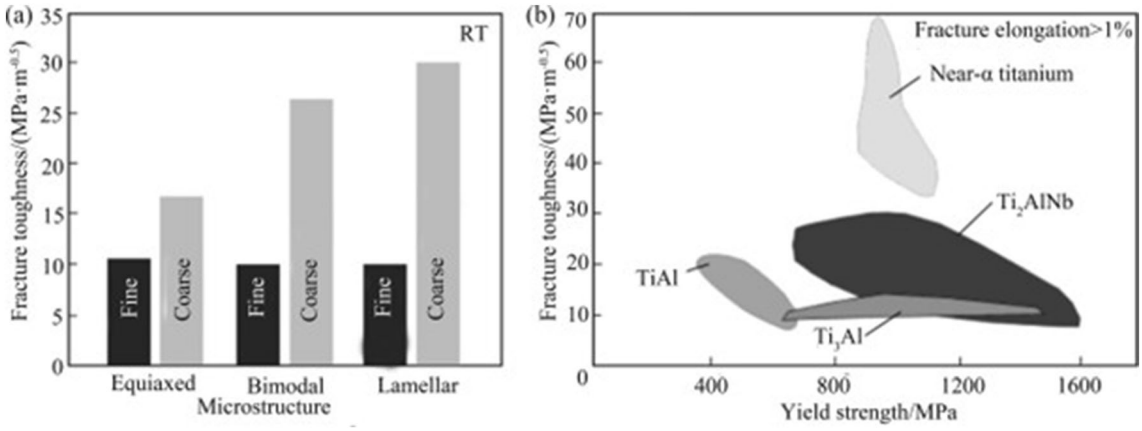

Fig. 26 (a) Fracture toughness of Ti_2AlNb alloy (Ref 5), (b) Fracture toughness vs. yield strength of Ti_2AlNb, near-α titanium, Ti_3Al, TiAl (Ref 5). Reprinted from J. Kumpfert, Intermetallic Alloys Based on Orthorhombic Titanium Aluminide, *Advanced Engineering Materials,* John Wiley and Sons. © 2001 WILEY-VCH Verlag GmbH, Weinheim, Fed. Rep. of Germany

precipitation of the α phase at grain boundaries influenced the mechanical properties of the alloy, and the morphology, size, and distribution state of the α phase had different effects on the alloy. By optimizing the microstructural morphology, different deformation processes can alter the mechanical properties of the alloy.

Fracture toughness (Ref 148) reflects the material's resistance to crack unstable propagation and is an important assessment criterion in aircraft damage tolerance design, directly affecting the aircraft's lifespan. The fracture toughness of this alloy is significantly related to the microstructural state, as shown in Fig. 26. Alloy composition, grain size, and lamellar microstructure have a significant impact on the fracture toughness of the alloy. Alloy composition influences the fracture toughness. Higher Nb content and lower Al content can improve the alloy's cleavage fracture capability, while the substitution of Nb with Mo or Ta does not have a significant effect on fracture toughness (Ref 149). Decreasing grain size can enhance the material's fracture toughness. As shown in Fig. 26, the fracture toughness of this alloy depends on the microstructure, with the lamellar microstructure exhibiting the best fracture toughness (Ref 150). Moreover, the fracture toughness of the alloy is also related to the thickness of the lamellar microstructure, as an increase in lamellar thickness improves the fracture toughness. From the figure, it can also be observed that although the fracture toughness of this alloy is not as high as that of titanium alloys, it is better than other Ti-Al series alloys.

Creep resistance is a critical indicator for evaluating whether an alloy can be used in high-temperature environments of aircraft engines. Figure 27 shows a temperature comparison of different alloys when the total creep strain reaches 0.2% within 100 hours (Ref 151). It can be seen from the figure that the Ti-22Al-25Nb alloy exhibits good creep resistance within the range of 600-700 °C, which is attributed to its higher activation energy for grain boundary diffusion and lattice self-diffusion (Ref 152). The creep resistance of the alloy is closely related to alloy type, microstructural state, and grain size. After the addition of Mo and Zr, all three stages of creep resistance are superior to that of the Ti-22Al-27Nb alloy, which is attributed to the higher activation energy for lattice self-diffusion. The

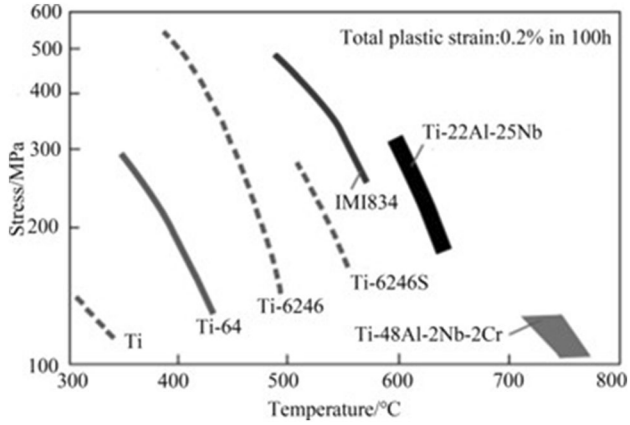

Fig. 27 Creep properties of Ti_2AlNb alloy and related alloys (Ref 151, 154)

creep deformation mechanism is controlled by dislocation climb. The addition of Zr can effectively enhance the alloy's creep resistance by coarsening the O-phase lamellae. He et al.'s study (Ref 153) found that the creep resistance is closely related to the proportion and morphology of the O-phase lamellae, with the O phase exhibiting higher creep resistance than the B2 phase. As the aging temperature increases, the thickness of the O-phase lamellae increases, leading to increased creep resistance. Therefore, the creep performance of the full lamellar microstructure is superior to the dual-phase microstructure. Boehlert et al.'s research (Ref 152) found that under low stress, the alloy exhibits low activation energy, with Coble creep being the dominant mechanism. Under moderate stress, grain boundary sliding and grain boundary diffusion occur, and the minimum creep rate is proportional to the square of the stress and inversely proportional to the grain size. Under high stress, the creep mechanism is controlled by dislocation climb. O-phase content is positively correlated with creep resistance.

Fatigue performance is another important indicator for studying this alloy. Currently, there are few research reports on the fatigue performance of this alloy, indicating a significant research gap in this field. As shown in Fig. 28, the high-cycle

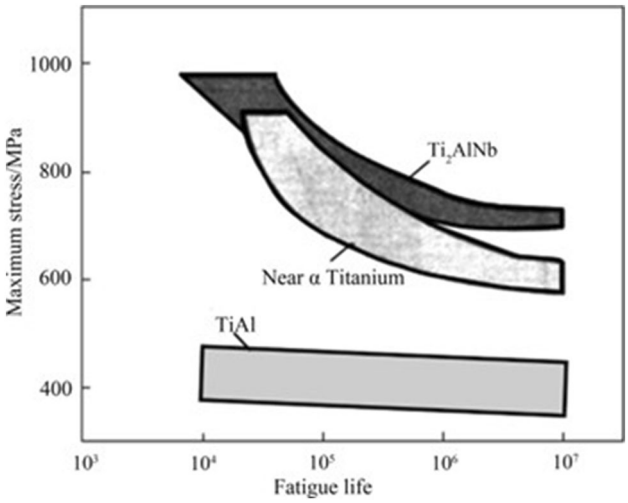

Fig. 28 High cycle fatigue of Ti_2AlNb alloy and related alloys (Ref 26). Reprinted from M. Peters and C. Leyens, *Titanium and Titanium Alloys: Fundamentals and Applications,* John Wiley & Sons. Copyright © 2003 Wiley-VCH Verlag GmbH & Co. KGaA

fatigue performance of this alloy is superior to that of near-α titanium alloys and TiAl alloys. The fatigue performance of the alloy is related to alloy elements, microstructural state, and surface treatment. Singh et al. (Ref 155) investigated the influence of Mo on the low-cycle fatigue performance of the alloy and found that the addition of Mo resulted in a more uniform microstructure and increased the alloy's low-cycle fatigue resistance. Studies (Ref 156) have also indicated that shot peening can introduce compressive stress, thereby improving fatigue strength and fatigue life. The microstructure primarily affects fatigue performance in three aspects: the O-phase lamellar impede dislocation propagation through the O/B2 phase interface, improving crack initiation resistance; the B2 phase lamellar passivate crack propagation, exhibiting higher high-cycle fatigue life; the TiB particles in the microstructure can enhance room temperature high-cycle fatigue performance, with small particles impeding dislocation motion, while large particles release stress concentration and hinder fatigue crack propagation.

In summary, the mechanical properties of the Ti_2AlNb alloy, including tensile performance, fracture toughness, creep resistance, and fatigue performance, are closely related to its microstructural features. Factors such as alloy composition, microstructural states, heat treatment processes, and deformation processes all influence its mechanical properties. Further research is needed to gain a deeper understanding of the relationship between mechanical properties and microstructure to drive the future development of this alloy.

7. Conclusion and Prospects

The Ti_2AlNb alloy is considered a potential contender for manufacturing high-temperature structural components as a replacement for high-temperature nickel-based alloys due to its outstanding creep resistance and oxidation performance at elevated temperatures. However, its widespread application is limited by inherent brittleness, large grain size, and other physical characteristics. Elemental composition, microstructure, fabrication and machining processes, and mechanical properties are critical factors restricting its application, and research in these areas is still relatively underdeveloped. Consequently, it is essential to provide a comprehensive summary and a forward-looking perspective on the relevant aspects of this alloy.

The mechanical performance of the alloy is closely related to its composition, and researchers have been exploring the influence of various alloying elements on its properties. Numerous research findings indicate that introducing different alloying elements, including Al, Nb, Mo, Zr, among others, can enhance specific physical properties of the alloy, making it more suitable for practical applications. Moreover, extensive research has focused on the binary and ternary phase diagrams of this alloy, with room for further investigation under specific conditions.

The alloy mainly comprises the O phase, α_2 phase, and B2 phase, with different combinations of phase content and morphology leading to three typical microstructures: bimodal, lamellar, and equiaxed structures. Due to the varying content and morphology characteristics of these phases, they exhibit distinct mechanical properties, with bimodal microstructures demonstrating superior comprehensive mechanical performance. Currently, methods for microstructure control of the alloy include heat treatment, plastic deformation, and controlling sintering parameters. In addition to traditional machining and manufacturing processes such as casting and welding, new manufacturing methods like additive manufacturing and powder metallurgy have garnered considerable attention among researchers. These novel methods offer numerous advantages, including exceptional material utilization, reduced processing steps, and enhanced production flexibility, when compared to traditional manufacturing methods.

The mechanical properties of the alloy, such as tensile and fracture performance, are closely linked to its microstructural state. Despite extensive research in this area, understanding the micro-mechanisms remains a primary focus for future investigations.

In conclusion, this article provides viable recommendations across four key aspects of the alloy: elemental composition, microstructure, manufacturing processes, and mechanical properties. While extensive research has been conducted in these four areas, there are still crucial issues that need to be addressed to promote the industrial application of this alloy. Future research should emphasize the following aspects: 1. In-depth exploration of the microstructure, including microstructural morphology, formation mechanisms, and the relationship between microstructure and mechanical performance. Researchers should aim to establish the link between microstructure and relevant mechanical properties under various operational conditions. 2. Intensified research into the transformation mechanisms of the O-phase, especially at different temperatures. Despite some existing research on the deformation mechanisms of the O-phase at various temperatures, the available data remains limited and often lacks precision. 3. Continued exploration of emerging processing techniques such as additive manufacturing and powder metallurgy. The introduction of new processing methods, such as the powder bed fusion additive manufacturing technique, provides a high level of flexibility for the production of this alloy, reducing production steps and enhancing material usage efficiency.

However, research on these new processing methods for the alloy is still relatively scarce and is expected to become a hot topic in future alloy studies.

Acknowledgment

This research did not receive any specific grant from funding agencies in the public, commercial, or not-for-profit sectors.

References

1. D. Banerjee, A. Gogia, T. Nandi, and V. Joshi, A New Ordered Orthorhombic Phase in a Ti3AlNb Alloy, *Acta Metall.*, 1988, **36**(4), p 871–882
2. H. Zhang, N. Yan, H. Liang, and Y. Liu, Phase Transformation and Microstructure Control of Ti_2AlNb-Based Alloys: A Review, *J. Mater. Sci. Technol.*, 2021, **80**, p 203–216
3. K. Goyal and N. Sardana, Mechanical Properties of the Ti_2AlNb Intermetallic: A Review, *Trans. Indian Inst. Met.*, 2021, **74**(8), p 1839–1853
4. A. Illarionov, S. Stepanov, I. Naschetnikova, A. Popov, P. Soundappan, K. Raman, and S. Suwas, A Review—Additive Manufacturing of Intermetallic Alloys Based on Orthorhombic Titanium Aluminide Ti_2AlNb, *Materials*, 2023, **16**(3), p 991
5. J. Kumpfert, Intermetallic Alloys Based on Orthorhombic Titanium Aluminide, *Adv. Eng. Mater.*, 2001, **3**(11), p 851–864
6. A. Gogia, T. Nandy, D. Banerjee, T. Carisey, J. Strudel, and J. Franchet, Microstructure and Mechanical Properties of Orthorhombic Alloys in the Ti-Al-Nb System, *Intermetallics*, 1998, **6**(7–8), p 741–748
7. B. Lu, R. Yang, Y. Cui, and D. Li, A Comparison Study of Microstructure and Mechanical Properties of Ti-24Al-14Nb-3V-0.5 Mo with and Without Si, *Metall. Mater. Trans. A*, 2000, **31**, p 2205–2217
8. Y. Zhang, Q. Cai, Z. Ma, C. Li, L. Yu, and Y. Liu, Solution Treatment for Enhanced Hardness in Mo-Modified Ti_2AlNb-Based Alloys, *J. Alloys Compd.*, 2019, **805**, p 1184–1190
9. D. Wei, J. Li, T. Zhang, and H. Kou, Oxidation Behavior of Zr-Containing Ti_2AlNb-Based Alloy at 800 °C, *Trans. Nonferrous Met. Soc. China*, 2015, **25**(3), p 783–790
10. L. Germann, D. Banerjee, J. Guédou, and J. Strudel, Effect of Composition on the Mechanical Properties of Newly Developed Ti_2AlNb-Based Titanium Aluminide, *Intermetallics*, 2005, **13**(9), p 920–924
11. Y. Mao, M. Hagiwara, and S. Emura, Creep Behavior and Tensile Properties of Mo-and Fe-Added Orthorhombic Ti-22Al-11Nb-2Mo-1Fe Alloy, *Scripta Materialia*, 2007, **57**(3), p 261–264
12. A. Illarionov, S. Demakov, F. Vodolazskiy, S. Stepanov, S. Illarionova, M. Shabanov, and A. Popov, Alloys Based on Orthorhombic Intermetallic Ti_2AlNb: Phase Composition, *Alloy. Struct. Prop. Metall.*, 2023, **67**(3), p 305–323
13. F. Tang, S. Nakazawa, and M. Hagiwara, The Effect of Quaternary Additions on the Microstructures and Mechanical Properties of Orthorhombic Ti_2AlNb-Based Alloys, *Mater. Sci. Eng. A*, 2002, **329**, p 492–498
14. G. Chen, X. Wang, K. Ni, S. Hao, J. Cao, J. Ding, and X. Zhang, Investigation on the 1000, 1150 and 1400 °C Isothermal Section of the Ti-Al-Nb System, *Intermetallics*, 1996, **4**(1), p 13–22
15. S. Xu, X. Ding, Y. Xu, Y. Liang, X. Xu, T. Ye, J. He, and J. Lin, Phase Equilibria of the Ti-Al-Nb System at 1400 °C, *J. Alloys Compd.*, 2018, **730**, p 270–278
16. S. Xu, Y. Xu, Y. Liang, X. Xu, S. Gao, Y. Wang, J. He, and J. Lin, Phase Equilibria of the Ti-Al-Nb System at 1300 °C, *J. Alloys Compd.*, 2017, **724**, p 339–347
17. V. Witusiewicz, A. Bondar, U. Hecht, and T. Velikanova, The Al-B-Nb-Ti System: IV. Experimental Study and Thermodynamic Re-Evaluation of the Binary Al-Nb and Ternary Al-Nb-Ti Systems, *J. Alloys Compd.*, 2009, **472**(1), p 133–161
18. U. Kattner and W. Boettinger, Thermodynamic Calculation of the Ternary Ti-Al-Nb System, *Mater. Sci. Eng. A*, 1992, **152**(1), p 9–17
19. D. Cupid, O. Fabrichnaya, O. Rios, F. Ebrahimi, and H. Seifert, Thermodynamic Re-assessment of the Ti-Al-Nb System, *Int. J. Mater. Res.*, 2009, **100**(2), p 218–233
20. S. Xu, X. Xu, Y. Xu, Y. Liang, and J. Lin, Phase Transformations and Phase Equilibria of a Ti-46.5Al-16.5Nb Alloy, *Mater. Des.*, 2016, **101**, p 88–94
21. C. Boehlert, B. Majumdar, V. Seetharaman, and D. Miracle, Part I. The Microstructural Evolution in Ti-Al-Nb O+ BCC Orthorhombic Alloys, *Metall. Mater. Trans. A*, 1999, **30**, p 2305–2323
22. N. Kazantseva and S. Lepikhin, Study of the Ti-Al-Nb Phase Diagram, *Phys. Met. Metallogr.*, 2006, **102**, p 169–180
23. B. Wu, M. Zinkevich, F. Aldinger, M. Chu, and J. Shen, Prediction of the Ordering Behaviours of the Orthorhombic Phase Based on Ti_2AlNb Alloys by Combining Thermodynamic Model with ab Initio Calculation, *Intermetallics*, 2008, **16**(1), p 42–51
24. K. Muraleedharan, A. Gogia, T. Nandy, D. Banerjee, and S. Lele, Transformations in a Ti-24AI-15Nb Alloy: Part I. Phase Equilibria and Microstructure, *Metall. Mater. Trans. A*, 1992, **23**(2), p 401–415
25. K. Muraleedharan, T. Nandy, D. Banerjee, and S. Lele, Transformations in a Ti-24Al-15Nb Alloy: Part II. A Composition Invariant βo → O Transformation, *Metall. Trans. A*, 1992, **23**(2), p 417–431
26. M. Peters., C. Leyens., Titanium and Titanium Alloys: Fundamentals and Applications. Wiley, New York (2003)
27. D. Banerjee, The Intermetallic Ti_2AlNb, *Progress Mater. Sci.*, 1997, **42**(1), p 135–158
28. H. Zhang, Y. Zhang, H. Liang, L. Yu, and Y. Liu, Effect of the Primary O Phase on Thermal Deformation Behavior of a Ti_2AlNb-Based Alloy, *J. Alloys Compd.*, 2020, **846**, p 156458
29. H. Zhang, H. Li, Q. Guo, Y. Liu, and L. Yu, Hot Deformation Behavior of Ti-22Al-25Nb Alloy by Processing Maps and Kinetic Analysis, *J. Mater. Res.*, 2016, **31**(12), p 1764–1772
30. K. Muraleedharan, T.K. Nandy, D. Banerjee, and S. Lele, Phase Stability and Ordering Behaviour of the O Phase in Ti-Al-Nb Alloys, *Intermetallics*, 1995, **3**(3), p 187–199
31. S. van Bohemen, A. Kamp, R. Petrov, L. Kestens, and J. Sietsma, Nucleation and Variant Selection of Secondary α Plates in a β Ti Alloy, *Acta Materialia*, 2008, **56**(20), p 5907–5914
32. M. Salib, J. Teixeira, L. Germain, E. Lamielle, N. Gey, and E. Aeby-Gautier, Influence of Transformation Temperature on Microtexture Formation Associated with α Precipitation at β Grain Boundaries in a β Metastable Titanium Alloy, *Acta Materialia*, 2013, **61**(10), p 3758–3768
33. R. Shi, V. Dixit, H. Fraser, and Y. Wang, Variant Selection of Grain Boundary α by Special Prior β Grain Boundaries in Titanium Alloys, *Acta Materialia*, 2014, **75**, p 156–166
34. R. Shi, V. Dixit, G. Viswanathan, H. Fraser, and Y. Wang, Experimental Assessment of Variant Selection Rules for Grain Boundary α in Titanium Alloys, *Acta Materialia*, 2016, **102**, p 197–211
35. T. Furuhara, H. Nakamori, and T. Maki, Crystallography of α Phase Precipitated on Dislocations and Deformation Twin Boundaries in a β Titanium Alloy, Materials Transactions, *JIM (1952)*, 1992, **56**(9), p 1020–1029
36. N. Kazantseva, S. Demakov, and A. Popov, Microstructure and Plastic Deformation of Orthorhombic Titanium Aluminides Ti_2AlNb. III. Formation of Transformation Twins upon the B2 → O Phase Transformation, *Phys. Met. Metallogr.*, 2007, **103**(4), p 378–387
37. Y. Zhou, W. Li, D. Wang, L. Zhang, K. Ohara, J. Shen, T. Ebel, and M. Yan, Selective Laser Melting Enabled Additive Manufacturing of Ti-22Al-25Nb Intermetallic: Excellent Combination of Strength and Ductility, and Unique Microstructural Features Associated, *Acta Materialia*, 2019, **173**, p 117–129
38. L. Bendersky and W. Boettinger, Phase Transformations in the (Ti, Nb) 3 Al Section of the Ti-Al-Nb System—II. Experimental Tem Study of Microstructures, *Acta metallurgica et materialia*, 1994, **42**(7), p 2337–2352
39. F. Sadi and C. Servant, On the B2 → O Phase Transformation in Ti-Al-Nb Alloys, *Mater. Sci. Eng. A*, 2003, **346**(1), p 19–28
40. W. Wang, W. Zeng, D. Li, B. Zhu, Y. Zheng, and X. Liang, Microstructural evolution and tensile behavior of Ti_2AlNb alloys based α2-phase decomposition, *Mater. Sci. Eng. A*, 2016, **662**, p 120
41. Z. Huang, P. Lin, and J. Shen, Origin of the O Phase and its Effect on the Mechanical Properties of Rolled Ti-22Al-25Nb Alloy Sheets, *Mater. High Temp.*, 2021, **38**(2), p 103–113

42. O. Khadzhieva, A. Illarionov, and A. Popov, Effect of Aging on Structure and Properties of Quenched Alloy Based on Orthorhombic Titanium Aluminide Ti_2AlNb, *Phys. Met. Metall.*, 2014, **115**(1), p 12–20
43. Y. Wu and S. Hwang, The Effect of Aging on Microstructure of the O-Phase in Ti-24Al-14Nb-3V-0.5Mo Alloy, *Mater. Lett.*, 2001, **49**(2), p 131–136
44. W. Wang, W. Zeng, C. Xue, X. Liang, and J. Zhang, Microstructure Control and Mechanical Properties from Isothermal Forging and Heat Treatment of Ti-22Al-25Nb (at.%) Orthorhombic Alloy, *Intermetallics*, 2015, **56**, p 79–86
45. J. Peng, S. Li, M. Yong, and X. Sun, Phase Transformation and Microstructures in Ti-Al-Nb-Ta System, *Mater. Lett.*, 2002, **53**(1–2), p 57–62
46. W. Wang, W. Zeng, C. Xue, X. Liang, and J. Zhang, Microstructural Evolution, Creep, and Tensile Behavior of a Ti-22Al-25Nb (at.%) Orthorhombic Alloy, *Mater. Sci. Eng. A*, 2014, **603**, p 176–184
47. C. Xue, W. Zeng, W. Wang, X. Liang, and J. Zhang, Quantitative Analysis on Microstructure Evolution and Tensile Property for the Isothermally Forged Ti_2AlNb Based Alloy During Heat Treatment, *Mater. Sci. Eng. A*, 2013, **573**, p 183
48. W. Wang, W. Zeng, C. Xue, X. Liang, and J. Zhang, Quantitative Analysis of the Effect of Heat Treatment on Microstructural Evolution and Microhardness of an Isothermally Forged Ti-22Al-25Nb (at.%) Orthorhombic Alloy, *Intermetallics*, 2014, **45**, p 29–37
49. M. Li, Q. Cai, Y. Liu, Z. Ma, Z. Wang, Y. Huang, and H. Li, Formation of Fine B2/β+O Structure and Enhancement of Hardness in the Aged Ti_2AlNb-Based Alloys Prepared by Spark Plasma Sintering, *Metall. Mater. Trans. A*, 2017, **48**(9), p 4365
50. M. Hagiwara, S. Emura, A. Araoka, Y. Seung, and N. Woo, The Effect of Lamellar Morphology on Tensile and High-Cycle Fatigue Behavior of Orthorhombic Ti-22Al-27Nb Alloy, *Metall. Mater. Trans. A*, 2004, **35**(7), p 2161–2170
51. Y. Zhang, Q. Cai, and Y. Liu, Formation of Diverse B2+O Structure and Hardness of Mo-Modified Ti-22Al-25Nb Alloys Upon Cooling, *Vacuum*, 2019, **165**, p 199–206
52. Q. Han, X. Lei, H. Yang, X. Yang, Z. Su, S. Rui, N. Wang, X. Ma, H. Cui, and H. Shi, Effects of Temperature and Load on Fretting Fatigue Induced Geometrically Necessary Dislocation Distribution in Titanium Alloy, *Mater. Sci. Eng. A*, 2021, **800**, p 140308
53. Q. Han, S. Rui, W. Qiu, Y. Su, X. Ma, Z. Su, H. Cui, and H. Shi, Effect of Crystal Orientation on the Indentation Behaviour of Ni-Based Single Crystal Superalloy, *Mater. Sci. Eng. A*, 2020, **773**, p 138893
54. J. Yang, G. Wang, X. Jiao, Y. Li, and K. Zhang, Dynamic Spheroidisation Behaviour of the Lamellar Ti-22Al-25Nb Alloy During Hot Compression, *Mater. Sci. Technol.*, 2018, **34**(8), p 961–967
55. C. Boehlert, The Effects of Forging and Rolling on Microstructure in O+BCC Ti-Al-Nb Alloys, *Mater. Sci. Eng. A*, 2000, **279**(1), p 118–129
56. H. Zhang, C. Li, Z. Ma, L. Yu, H. Li, and Y. Liu, Morphology and Quantitative Analysis of O Phase During Heat Treatment of Hot-Deformed Ti_2AlNb-Based Alloy, *Int. J. Miner. Metall. Mater*, 2018, **25**(10), p 1191–1200
57. J. Yang, G. Wang, W. Zhang, W. Chen, X. Jiao, and K. Zhang, Microstructure Evolution and Mechanical Properties of P/M Ti-22Al-25Nb Alloy During Hot Extrusion, *Mater. Sci. Eng. A*, 2017, **699**, p 210–216
58. Y. Zhou, D. Wang, L. Song, A. Mukhtar, D. Huang, C. Yang, and M. Yan, Effect of Heat Treatments on the Microstructure and Mechanical Properties of Ti_2AlNb Intermetallic Fabricated by Selective Laser Melting, *Mater. Sci. Eng. A*, 2021, **817**, p 141352
59. X. Yang, B. Zhang, Q. Bai, and G. Xie, Correlation of Microstructure and Mechanical Properties of Ti_2AlNb Manufactured by SLM and Heat Treatment, *Intermetallics*, 2021, **139**, p 107367
60. C. Xue, W. Zeng, W. Wang, X. Liang, and J. Zhang, Quantitative Analysis on Microstructure Evolution and Tensile Property for the Isothermally Forged Ti_2AlNb Based Alloy During Heat Treatment, *Mater. Sci. Eng. A*, 2013, **573**, p 183–189
61. Y. He, R. Hu, W. Luo, T. He, Y. Lai, Y. Du, and X. Liu, Microstructure and Mechanical Properties of a New Ti_2AlNb-Based Alloy After Aging Treatment, *Rare Metals*, 2018, **37**(11), p 942–951
62. Y. Huang, Y. Liu, Y. Zhang, and H. Liang, Thermal Stability and Mechanical Properties of Ti-22Al-25Nb Alloy with Different Initial Microstructures, *J. Alloys. Compd.*, 2020, **842**, p 155794
63. H. Zhang, Y. Zhang, H. Liang, and Y. Liu, Influence of Cooling Rates on Microstructure and Tensile Properties of a Heat Treated Ti_2AlNb-Based Alloy, *Mater. Sci. Eng. A*, 2021, **817**, p 141345
64. Z. Bu, Y. Zhang, L. Yang, J. Kang, and J. Li, Effect of Cooling Rate on Phase Transformation in Ti_2AlNb Alloy, *J. Alloys Compd.*, 2022, **893**, p 162364
65. H. Zhang, C. Li, Z. Ma, Y. Huang, L. Yu, and Y. Liu, Static Coarsening Behavior of a Pre-deformed Ti_2AlNb-Based Alloy During Heat Treatment, *Vacuum*, 2019, **169**, p 108934
66. X. Chen, W. Zeng, W. Wang, X. Liang, and J. Zhang, Coarsening Behavior of Lamellar Orthorhombic Phase and its Effect on Tensile Properties for the Ti-22Al-25Nb Alloy, *Mater. Sci. Eng. A*, 2014, **611**, p 320–325
67. G. Wang, J. Yang, and X. Jiao, Microstructure and Mechanical Properties of Ti-22Al-25Nb Alloy Fabricated by Elemental Powder Metallurgy, *Mater. Sci. Eng. A*, 2016, **654**, p 69–76
68. Y. Wang, K. Zhang, and B. Li, Microstructure and High Temperature Tensile Properties of Ti22Al25Nb Alloy Prepared by Reactive Sintering with Element Powders, *Mater. Sci. Eng. A*, 2014, **608**, p 229–233
69. Z. Yang, H. Liu, Z. Cui, H. Zhang, and F. Chen, Refinement Mechanism of Centimeter-Grade Coarse Grains in As-Cast Ti_2AlNb-Based Alloy During Multi-directional Forging, *Mater. Des.*, 2023, **225**, p 111508
70. C. Boehlert, The Effects of Forging and Rolling on Microstructure in O + BCC Ti-Al-Nb Alloys, *Mater. Sci. Eng. A*, 2000, **279**(1/2), p 279
71. D. Miracle and O. Senkov, A Critical Review of High Entropy Alloys and Related Concepts, *Acta Materialia*, 2017, **122**, p 448–511
72. X. Sauvage, G. Wilde, S. Divinski, Z. Horita, and R. Valiev, Grain Boundaries in Ultrafine Grained Materials Processed by Severe Plastic Deformation and Related Phenomena, *Mater. Sci. Eng. A*, 2012, **540**, p 1–12
73. K. Kumar, H. Van Swygenhoven, and S. Suresh, Mechanical Behavior of Nanocrystalline Metals and Alloys, *Acta Materialia*, 2003, **51**(19), p 5743–5774
74. R. Valiev and T. Langdon, Principles of Equal-Channel Angular Pressing as a Processing Tool for Grain Refinement, *Progress Mater. Sci.*, 2006, **51**(7), p 881–981
75. N. Azizi, and R. Mahmudi, Microstructure, Texture, and Mechanical Properties of the Extruded and Multi-directionally Forged Mg-xGd Alloys, *Mater. Sci. Eng. A*, 2021, **817**, p 141385
76. Z. Yang, H. Liu, Z. Cui, H. Zhang, and F. Chen, Refinement Mechanism of Centimeter-Grade Coarse Grains in As-Cast Ti_2AlNb-Based Alloy During Multi-Directional Forging, *Mater. Des.*, 2023, **225**, p 111508
77. J. Peng, Y. Mao, S. Li, and X. Sun, Microstructure Controlling by Heat Treatment and Complex Processing for Ti_2AlNb Based Alloys, *Mater. Sci. Eng. A*, 2001, **299**(1–2), p 75–80
78. Y. Wu, C. Yang, C. Koo, and A. Singh, A Study of Texture and Temperature Dependence of Mechanical Properties in Hot Rolled Ti-25Al-xNb Alloys, *Mater. Chem. Phys.*, 2003, **80**(1), p 339–347
79. S. Semiatin and P. Smith, Microstructural Evolution During Rolling of Ti-22Al-23Nb Sheet, *Mater. Sci. Eng. A*, 1995, **202**(1), p 26–35
80. S. Dey, S. Suwas, J. Fundenberger, J. Zou, T. Grosdidier, and R. Ray, Evolution of Hot Rolling Texture in β (B2)-Phase of a Two-Phase (O+B2) Titanium-Aluminide Alloy. Mater. Sci. Eng. A, 2008, **483–484**(12), p 551–554
81. S. Emura, A. Araoka, and M. Hagiwara, B2 Grain Size Refinement and its Effect on Room Temperature Tensile Properties of a Ti-22Al-27Nb Orthorhombic Intermetallic Alloy, *Scripta Materialia*, 2003, **48**(5), p 629–634
82. J. Xu, L. He, H. Su, and L. Zhang, Tool Wear Investigation in High-Pressure Jet Coolant Assisted Machining Ti_2AlNb Intermetallic Alloys Based on FEM, *Int. J. Lightweight Mater. Manuf.*, 2018, **1**(4), p 219–228
83. L. He, H. Su, J. Xu, and L. Zhang, Study on Dynamic Chip Formation Mechanisms of Ti_2AlNb Intermetallic Alloy, *Int. J. Adv. Manuf. Technol*, 2017, **92**, p 4415–4428
84. F. Nabhani, Wear Mechanisms of Ultra-Hard Cutting Tools Materials, *J. Mater. Process. Technol.*, 2001, **115**(3), p 402–412

85. D. Zhu, X. Zhang, and H. Ding, Tool Wear Characteristics in Machining of Nickel-Based Superalloys, *Int. J. Mach. Tools Manuf.*, 2013, **64**, p 60–77
86. E. Ezugwu, R. Silva, J. Bonney, and Á. Machado, Evaluation of the Performance of CBN Tools When Turning Ti-6Al-4V Alloy with High Pressure Coolant Supplies, *Int. J. Mach. Tools Manuf.*, 2005, **45**(9), p 1009–1014
87. A. Machado, J. Wallbank, I. Pashby, and E. Ezugwu, Tool Performance and Chip Control when Machining Ti6Al4V and Inconel 901 Using High Pressure Coolant Supply, *Mach. Sci. Technol.*, 1998, **2**(1), p 1–12
88. M. Habak and J. Lebrun, An Experimental Study of the Effect of High-Pressure Water Jet Assisted Turning (HPWJAT) on the Surface Integrity, *Int. J. Mach. Tools Manuf.*, 2011, **51**(9), p 661–669
89. E. Ezugwu and J. Bonney, Effect of High-Pressure Coolant Supply when Machining Nickel-Base, Inconel 718, Alloy with Coated Carbide Tools, *J. Mater. Process. Technol.*, 2004, **153–154**, p 1045–1050
90. E. Ezugwu and J. Bonney, Finish Machining of Nickel-Base Inconel 718 Alloy with Coated Carbide Tool under Conventional and High-Pressure Coolant Supplies, *Tribol. Trans.*, 2005, **48**(1), p 76–81
91. M. Bermingham, S. Palanisamy, D. Kent, and M. Dargusch, A Comparison of Cryogenic and High Pressure Emulsion Cooling Technologies on Tool Life and Chip Morphology in Ti-6Al-4V Cutting, *J. Mater. Process. Technol.*, 2012, **212**(4), p 752–765
92. D. Kramar, P. Krajnik, and J. Kopac, Capability of High Pressure Cooling in the Turning of Surface Hardened Piston Rods, *J. Mater. Process. Technol.*, 2010, **210**(2), p 212–218
93. A. Hadzley, R. Izamshah, A. Sarah, and M. Fatin, Finite Element Model of Machining with High Pressure Coolant for Ti-6Al-4V Alloy, *Procedia Eng.*, 2013, **53**, p 624–631
94. J. Kaminski, O. Ljungkrona, R. Crafoord, and S. Lagerberg, Control of Chip Flow Direction in High-Pressure Water Jet-Assisted Orthogonal Tube Turning, *Proc. Inst. Mech. Eng. Part B J. Eng. Manuf.*, 2000, **214**(7), p 529–534
95. M. Calamaz, D. Coupard, and F. Girot, A New Material Model for 2D Numerical Simulation of Serrated Chip Formation when Machining Titanium Alloy Ti-6Al-4V, *Int. J. Mach. Tools Manuf.*, 2008, **48**(3), p 275–288
96. X. Chen, F. Xie, T. Ma, W. Li, and X. Wu, Effects of Post-Weld Heat Treatment on Microstructure and Mechanical Properties of Linear Friction Welded Ti_2AlNb Alloy, *Mater. Des.*, 2016, **94**, p 45–53
97. X. Chen, F. Xie, T. Ma, W. Li, and X. Wu, Microstructural Evolution and Mechanical Properties of Linear Friction Welded Ti_2AlNb Joint During Solution and Aging Treatment, *Mater. Sci. Eng. A*, 2016, **668**, p 125–136
98. Y. Chen, K. Zhang, X. Hu, Z. Lei, and L. Ni, Study on Laser Welding of a Ti-22Al-25Nb Alloy: Microstructural Evolution and High Temperature Brittle Behavior, *J. Alloys Compd.*, 2016, **681**, p 175–185
99. K. Zhang, L. Ni, Z. Lei, Y. Chen, and X. Hu, Microstructure and Tensile Properties of Laser Welded Dissimilar Ti-22Al-27Nb and TA15 Joints, *Int. J. Adv. Manuf. Technol.*, 2016, **87**, p 1685–1692
100. Z. Lei, Z. Dong, Y. Chen, J. Zhang, and R. Zhu, Microstructure and Tensile Properties of Laser Beam Welded Ti-22Al-27Nb Alloys, *Mater. Des. (1980–2015)*, 2013, **46**, p 151–156
101. L. Tan, Z. Yao, Y. Ning, and H. Guo, Effect of Isothermal Deformation on Microstructure and Properties of Electron Beam Welded Joint of Ti_2AlNb/TC11, *Mater. Sci. Technol.*, 2011, **27**(9), p 1469–1474
102. L. Tan, Z. Yao, T. Wang, and H. Guo, Effect of Post-Weld Heat Treatment on Microstructure and Properties of Electron Beam Welded Joint of Ti_2AlNb/TC11, *Mater. Sci. Technol.*, 2011, **27**(8), p 1315–1320
103. L. Tan, Z. Yao, W. Zhou, H. Guo, and Y. Zhao, Microstructure and Properties of Electron Beam Welded Joint of Ti-22Al-25Nb/TC11, *Aerosp. Sci. Technol.*, 2010, **14**(5), p 302–306
104. G. Zou, E. Xie, H. Bai, A. Wu, Q. Wang, and J. Ren, A Study on Transient Liquid Phase Diffusion Bonding of Ti-22Al-25Nb Alloy, *Mater. Sci. Eng. A*, 2009, **499**(1), p 101–105
105. Z. Lei, Z. Dong, Y. Chen, L. Huang, and R. Zhu, Microstructure and Mechanical Properties of Laser Welded Ti-22Al-27Nb/TC4 Dissimilar Alloys, *Mater. Sci. Eng. A*, 2013, **559**, p 909–916
106. P. Ferro, A. Zambon, and F. Bonollo, Investigation of Electron-Beam Welding in Wrought Inconel 706—Experimental and Numerical Analysis, *Mater. Sci. Eng. A*, 2005, **392**(1), p 94–105
107. X. Chen, F. Xie, T. Ma, W. Li, and X. Wu, Oxidation Behavior of Three Different Zones of Linear Friction Welded Ti_2AlNb Alloy, *Adv. Eng. Mater.*, 2016, **18**(11), p 1944–1951
108. S. Wang, J. Liu, and D. Chen, Tensile and Fatigue Properties of Electron Beam Welded Dissimilar Joints Between Ti-6Al-4V and BT9 Titanium Alloys, *Mater. Sci. Eng. A*, 2013, **584**, p 47–56
109. J. Sabol, T. Pasang, W. Misiolek, and J. Williams, Localized Tensile Strain Distribution and Metallurgy of Electron Beam Welded Ti-5Al-5V-5Mo-3Cr Titanium Alloys, *J. Mater. Process. Technol.*, 2012, **212**(11), p 2380–2385
110. H. Niu, Y. Chen, D. Zhang, Y. Zhang, J. Lu, W. Zhang, and P. Zhang, Fabrication of a Powder Metallurgy Ti_2AlNb-Based Alloy by Spark Plasma Sintering and Associated Microstructure Optimization, *Mater. Des.*, 2016, **89**, p 823–829
111. K. Rao, Y. Prasad, and K. Suresh, Hot Working Behavior and Processing Map of a γ-TiAl Alloy Synthesized by Powder Metallurgy, *Mater. Des.*, 2011, **32**(10), p 4874–4881
112. Y. Wang, J. Lin, X. Xu, Y. He, Y. Wang, and G. Chen, Effect of Fabrication Process on Microstructure of High Nb Containing TiAl Alloy, *J. Alloys Compd.*, 2008, **458**(1), p 313–317
113. N. Zhang, X. Han, D. Sun, S. Liu, H. Liu, W. Yang, and G. Wu, Microstructure Evolution and Mechanical Properties of LaB6-Modified Ti_2AlNb Alloy Fabricated By Blended Elemental Powder Metallurgy, *Powder Technol.*, 2020, **369**, p 334–344
114. C. Yolton and J. Beckman, Powder Metallurgy Processing and Properties of the Ordered Orthorhombic Alloy Ti-22at.%Al-23at.%Nb, *Mater. Sci. Eng. A*, 1995, **192**, p 597–603
115. N. Zhang, D. Sun, X. Han, Z. Wang, H. Liu, Z. Wang, W. Yang, and G. Wu, Effect of Spark Plasma Sintering Temperatures on Microstructure and Mechanical Properties of In-Situ (La_2O_3+TiB)/Ti_2AlNb Composites with a Tailored Three-Dimensional Network Architecture, *Mater. Sci. Eng. A*, 2020, **772**, p 138769
116. J. Wu, R. Guo, L. Xu, Z. Lu, Y. Cui, and R. Yang, Effect of Hot Isostatic Pressing Loading Route on Microstructure and Mechanical Properties of Powder Metallurgy Ti_2AlNb Alloys, *J. Mater. Sci. Technol.*, 2017, **33**(2), p 172–178
117. K. Sim, G. Wang, R. Son, and S. Choe, Influence of Mechanical Alloying on the Microstructure and Mechanical Properties of Powder Metallurgy Ti_2AlNb-Based Alloy, *Powder Technol.*, 2017, **317**, p 133–141
118. K. Sim, G. Wang, Y. Li, and J. Jong, Enhanced Ductility of a Bimodal Grain Structure Ti-22Al-25Nb Alloy Fabricated by Spark Plasma Sintering, *Adv. Eng. Mater.*, 2017, **19**(6), p 1600804
119. Y. Wang, Z. Lu, K. Zhang, and D. Zhang, Thermal Mechanical Processing Effects on Microstructure Evolution and Mechanical Properties of the Sintered Ti-22Al-25Nb Alloy, *Materials*, 2016, **9**(3), p 189
120. B. Shao, S. Wan, W. Xu, D. Shan, B. Guo, and Y. Zong, Formation Mechanism of an α2 Phase-Rich Layer on the Surface of Ti-22Al-25Nb Alloy, *Mater. Charact.*, 2018, **145**, p 205–209
121. M. Yan, M. Dargusch, T. Ebel, and M. Qian, A Transmission Electron Microscopy and Three-Dimensional Atom Probe Study of the Oxygen-Induced Fine Microstructural Features in As-Sintered Ti-6Al-4V and Their Impacts on Ductility, *Acta Materialia*, 2014, **68**, p 196–206
122. C. Rhodes, P. Smith, W. Hanusiak, and M. Shepard, Microstructural Evolution in Wire-Drawn Ti-22Al-26Nb Powder, *Metall. Mater. Trans. A*, 2000, **31**(11), p 2931–2941
123. M. Yan, W. Xu, M.S. Dargusch, H.P. Tang, M. Brandt, and M. Qian, Review of Effect of Oxygen on Room Temperature Ductility of Titanium and Titanium Alloys, *Powder Metall.*, 2014, **57**(4), p 251–257
124. J. Lou, B. Gabbitas, F. Yang, S. Raynova, and H. Lu, Effects of LaB6 Additions on the Microstructure and Mechanical Properties of a Sintered and Hot Worked P/M Ti Alloy, *J. Alloys Compd.*, 2016, **674**, p 116–124
125. A. Kartavykh, E. Asnis, N. Piskun, I. Statkevich, M. Gorshenkov, and V. Tcherdyntsev, Lanthanum Hexaboride as Advanced Structural Refiner/Getter in TiAl-Based Refractory Intermetallics, *J. Alloys Compd.*, 2014, **588**, p 122–126

126. M. Yan, Y. Liu, G. Schaffer, and M. Qian, In Situ Synchrotron Radiation to Understand the Pathways for the Scavenging of Oxygen in Commercially Pure Ti and Ti-6Al-4V by Yttrium Hydride, *Scripta Materialia*, 2013, **68**(1), p 63–66
127. Y. Yang, S. Luo, and M. Qian, The Effect of Lanthanum Boride on the Sintering, Sintered Microstructure and Mechanical Properties of Titanium and Titanium Alloys, *Mater. Sci. Eng. A*, 2014, **618**, p 447–455
128. J. Jia, K. Zhang, and S. Jiang, Microstructure and Mechanical Properties of Ti-22Al-25Nb Alloy Fabricated by Vacuum Hot Pressing Sintering, *Mater. Sci. Eng. A*, 2014, **616**, p 93–98
129. J. Groza and A. Zavaliangos, Sintering Activation by External Electrical Field, *Mater. Sci. Eng. A*, 2000, **287**(2), p 171–177
130. J. Wu, L. Xu, Z. Lu, B. Lu, Y. Cui, and R. Yang, Microstructure Design and Heat Response of Powder Metallurgy Ti_2AlNb Alloys, *J. Mater. Sci. Technol.*, 2015, **31**(12), p 1251–1257
131. I. Polozov, K. Starikov, A. Popovich, and V. Sufiiarov, Mitigating Inhomogeneity and Tailoring the Microstructure of Selective Laser Melted Titanium Orthorhombic Alloy by Heat Treatment, Hot Isostatic Pressing, and Multiple Laser Exposures, *Materials*, 2021, **14**, p 4946
132. I. Polozov, V. Sufiiarov, K. Starikov, and A. Popovich, In Situ Synthesized Ti_2AlNb-Based Composites Produced by Selective Laser Melting by Addition of SiC-Whiskers, *Mater. Lett.*, 2021, **297**, p 129956
133. J. Pragana, R. Sampaio, I. Bragança, C. Silva, and P. Martins, Hybrid Metal Additive Manufacturing: A State-of-the-Art Review, *Adv. Ind. Manuf. Eng.*, 2021, **2**, p 100032
134. I. Polozov, K. Starikov, A. Popovich, and V. Sufiiarov, Mitigating Inhomogeneity and Tailoring the Microstructure of Selective Laser Melted Titanium Orthorhombic Alloy by Heat Treatment, Hot Isostatic Pressing, and Multiple Laser Exposures, *Materials*, 2021, **14**(17), p 4946
135. S. Yang, S. Nam, and M. Hagiwara, Investigation of Creep Deformation Mechanisms and Environmental Effects on Creep Resistance in a Ti_2AlNb Based Intermetallic Alloy, *Intermetallics*, 2004, **12**(3), p 261–274
136. K. Miyoshi, B. Lerch, and S. Draper, Fretting Wear of Ti-48Al-2Cr-2Nb, *Tribol. Int.*, 2003, **36**(2), p 145–153
137. X. Liu, Z. Xu, W. Xu, W. Liang, C. Guo, and W. Tian, Plasma Surface Alloying with Molybdenum and Carburization of TiAl Based Alloys, *Trans. Nonferrous Met. Soc. China*, 2005, **15**(3), p 420–424
138. H. Wu, P. Zhang, J. Li, S. Ma, and Z. Xu, Microstructure and Tribological Properties of Surface Plasma Chromising Layer of Ti_2AlNb-Based Alloy, *Trans. Nonferrous Met. Soc. China*, 2007, **17**(10), p 1656–1660
139. A. Srivastava and K. Das, Microstructure and Abrasive Wear Study of (Ti, W)C-Reinforced High-Manganese Austenitic Steel Matrix Composite, *Mater. Lett.*, 2008, **62**(24), p 3947–3950
140. H. Wu and P. Zhang, Effect of W Substitution on Electronic Structures and Properties of Ti_2AlNb-Based Alloy, *Rare Metal Mater. Eng.*, 2007, **36**(5), p 846–848
141. T. Solzak and A. Polycarpou, Tribology of WC/C Coatings for Use in Oil-Less Piston-Type Compressors, *Surf. Coat. Technol.*, 2006, **201**(7), p 4260–4265
142. Y. Zhang, Y. Liu, L. Yu, H. Liang, Y. Huang, and Z. Ma, Microstructures and Tensile Properties of Ti_2AlNb and Mo-Modified Ti_2AlNb Alloys Fabricated by Hot Isostatic Pressing, *Mater. Sci. Eng. A*, 2020, **776**, p 139043
143. S. Li and Y. Mao, Effect of Microstructure on Tensile Properties and Fracture Behavior of Intermetallic Ti_2AlNb Alloys, *Trans. Nonferrous Met. Soc. China*, 2002, **12**(4), p 582–586
144. Y. Fu, M. Lv, Q. Zhao, H. Zhang, and Z. Cui, Investigation on the Size and Distribution Effects of O Phase on Fracture Properties of Ti_2AlNb Superalloy by Using Image-Based Crystal Plasticity Modeling, *Mater. Sci. Eng. A*, 2021, **805**, p 140787
145. Y. Fu and Z. Cui, Effects of Plastic Deformation and Aging Treatment on Phase Precipitation in Ti_2AlNb Alloy, *J. Mater. Eng. Perform.*, 2022, **31**(4), p 2633–2643
146. C. Boehlert, Part III. The Tensile Behavior of Ti-Al-Nb O+bcc Orthorhombic Alloys, *Metall. Mater. Trans. A*, 2001, **32**(8), p 1977–1988
147. J. Zhang, H. Zhang, X. Zhang, X. Liang, Y. Cheng, and S. Li, Control of Duplex-Microstructure and Its Effect on Mechanical Properties of Ti-23Al-17Nb Alloys, *Rare Metal Mater. Eng.*, 2010, **39**(2), p 372–376
148. C. Oskay, Z. Su, and B. Kapusuzoglu, Discrete Eigenseparation-Based Reduced Order Homogenization Method for Failure Modeling of Composite Materials, *Comput. Methods Appl. Mech. Eng.*, 2020, **359**, p 112656
149. S. Kamat, A. Gogia, and D. Banerjee, Effect of alloying elements and heat treatment on the fracture toughness of Ti-Al-Nb alloys, *Acta Materialia*, 1998, **46**(1), p 239–251
150. Z. Shi, H. Guo, J. Zhang, and J. Yin, Microstructure−Fracture Toughness Relationships and Toughening Mechanism of TC21 Titanium Alloy with Lamellar Microstructure, *Trans. Nonferrous Met. Soc. China*, 2018, **28**(12), p 2440–2448
151. M. Keller, P. Jones, W. Porter, D. Eylon, Effects of processing variables on the creep behavior of investment cast Ti-48Al-2Nb-2Cr. United States: Minerals, Metals and Materials Society, Warrendale, PA (United States), United States, 1995
152. C. Boehlert and D. Miracle, Part II. The Creep Behavior of Ti-Al-Nb O + Bcc orthorhombic alloys, *Metall. Mater. Trans. A*, 1999, **30**(9), p 2349–2367
153. Y. He, R. Hu, W. Luo, T. He, Y. Lai, Y. Du, and X. Liu, Microstructural Evolution and Creep Deformation Behavior of Novel Ti−22Al−25Nb−1Mo−1V−1Zr−02Si (at.%) Orthorhombic Alloy, *Trans. Nonferrous Met. Soc. China*, 2019, **29**(2), p 313–321
154. R. Boyer, G. Welsch, and E. Collings, *Materials Properties Handbook-Titanium Alloys*, ASM International, 1994
155. P. Singh, B. Singh, C. Ramachandra, and V. Singh, Room Temperature Low Cycle Fatigue Behaviour of Titanium Aluminide Ti-26.2Al-15.2Nb-0.4Mo, *Scripta Materialia*, 1996, **34**(11), p 1791–1796
156. Y. Chen, J. Wang, Y. Gao, and A. Feng, Effect of Shot Peening on Fatigue Performance of Ti_2AlNb Intermetallic Alloy, *Int. J. Fatigue*, 2019, **127**, p 53–57
157. Z. Yang, W. Liang, Q. Miao, B. Chen, Z. Ding, and N. Roy, Oxidation Behavior of Al/Cr Coating on Ti_2AlNb Alloy at 900 °C, *Mater. Res. Express*, 2018, **5**(4), p 046408